Migration and Stability of Multi-Planet Circumbinary Systems

Undergraduate Research Thesis

Presented in Partial Fulfillment of the Requirements for graduation *with Honors Research Distinction* in Astronomy in the undergraduate colleges of The Ohio State University

by

Evan Fitzmaurice

The Ohio State University

April 2021

Project Advisor: Dr. David V. Martin, Department of Astronomy

Thesis Advisor: Professor B. Scott Gaudi, Department of Astronomy

Draft version May 5, 2021
Typeset using LaTeX **manuscript** style in AASTeX63

ABSTRACT

Of the known circumbinary planets, most are single planets observed just outside of the zone of instability caused by gravitational interactions with the binary. Migration is the preferred mechanism of getting circumbinary planets to these positions, as the turbulent conditions in these zones make in situ planetary formation unlikely. Only one confirmed multi-planet circumbinary system is known in Kepler-47. In order to understand the stability and likelihood of multi-planet circumbinary systems, we have modeled currently known systems with synthetic outer planets using varying starting parameters. Our simulations indicate long-term stable resonant locking occurring most reliably for mass ratios (outer/inner) less than 0.1, with some exception up to 0.4. Systems below this threshold lock primarily in the 2:1 resonance, with occasional exception to the 3:2 resonance. Mass ratios greater than one and up to ten are probed, but these cases cause the inner planet to be pushed interior to the realm of instability, resulting in the ejection of the inner planet, and occasionally also the outer planet. Our results have implications on the potential discovery of additional planets in known single-planet circumbinary systems, an understanding of the transition between stable and unstable multi-planet architectures, and a source for free-floating exoplanets.

1. FOUNDATIONS

1.1. *Exoplanets*

Exoplanets are known as planets orbiting stars that are not our own. The first discovery of an exoplanet came in 1992, being found around the pulsar PSR1257 + 12 (Wolszczan & Frail 1992). While this jump started a pursuit for more discoveries, a surprising early discovery came in the existence of "hot Jupiters", Jupiter-like planets that orbit closely to their host star, and are thus hotter than Jupiter in our Solar System. The first hot Jupiter discovered was 51 Pegasi b (Mayor & Queloz 1995), which orbited a sun-like star. As older detection methods have been improved and

new ones created, the data set has exploded with more than 4,000 confirmed exoplanets being known to date. With this explosion has come a widening in the types of planets and system architectures found. From Earth-, Saturn-, and Neptune-like single planet systems, to multiple planets orbiting binary stars, the potential variety for discovery is seemingly limitless. This expansion of the discovery of exoplanets has led to a need to understand how planetary systems form and evolve over time.

While it may seem that we can find any and all types of planets in a variety of configurations, our data set is constrained by our ability to implement techniques to detect these planets. The most relevant detection methods to our topic are the *transit* and *radial velocity* methods. Each comes with limitations but are generally the most robust methods and are particularly powerful when used in conjunction.

1.1.1. *Transit Method*

The transit method requires the observation of the brightness of a star over a period of time, as portrayed by Figure 1. As we observe the star, if a planet's orbit is aligned such that it passes in between us and the star, it may cause a detectable dip in the observed brightness of the star, known as a *transit*. While the transit method has been used to discover the most exoplanets of any method, it comes with its own intrinsic observational bias. This method is most likely to detect large planets, since it requires a large enough planet to block enough starlight to be noticeable. There is also a bias towards systems with inclinations nearly at or equal to 90 degrees, referred to as 'edge on' systems. An edge on system means that the planet passes directly in line with our line of sight allowing us to see a transit. A non-edge on system means it completely misses so we would not see any dip in brightness. This inclination bias leads to a positive bias for the transit method to discover short period planets, as the geometry for these systems increases the probability of a transit occurring. Two of the biggest missions to discover planets via the transit method have been the *Kepler* and *TESS* missions. The transit method, specifically using Kepler, has built the foundation of circumbinary planet discoveries, identifying the first 10 systems. Several other candidate circumbinary planets exist from eclipse timing variations of post-common envelope binaries, but these are heavily disputed and not featured in our study (Bear & Soker 2014 ; Zorotovic & Schreiber 2013).

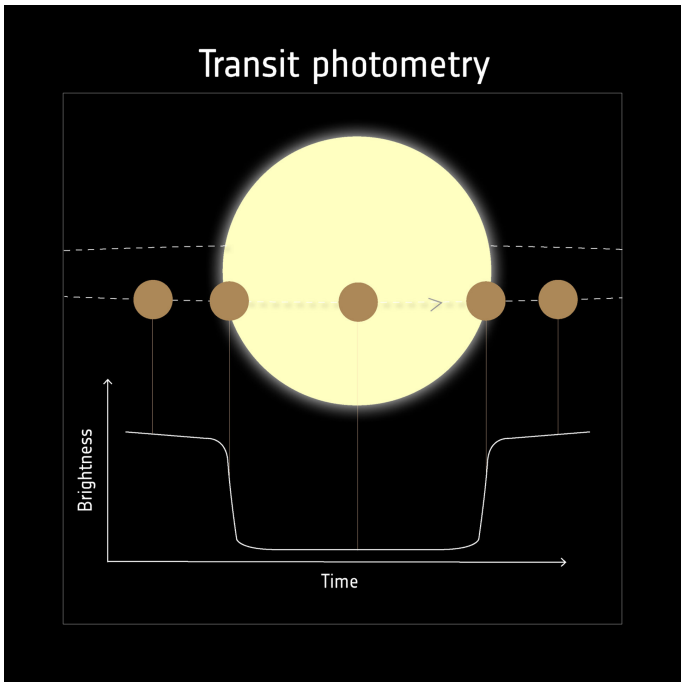

Figure 1. Graphic example of a planet transiting its host star and the corresponding features that would be seen in the lightcurve at each instance. Credit: European Space Agency (ESA)

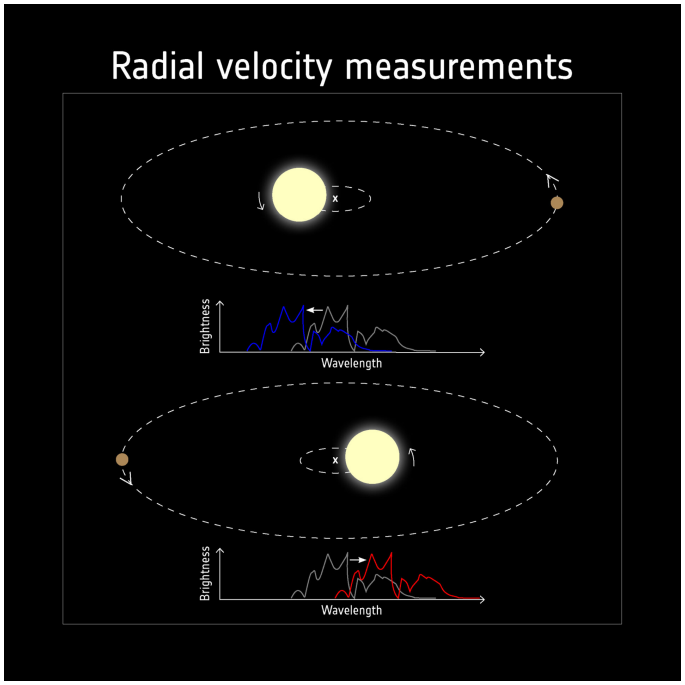

Figure 2. Graphic representation of blueshifting and redshifting of observed starlight when a planet is present, and how the position of the planet can be indicated by the type of shifting. Credit: ESA

1.1.2. *Radial Velocity Method*

The radial velocity (RV), or Doppler method, involves watching the spectra of a star over time, as shown in Figure 2. As we observe the absorption features of the star's spectrum, if a planet is present, these features will periodically become blue and red shifted. This is due to the fact that when a planet is present around the star, they both orbit around a center of mass and so this causes the star to periodically move away from and towards the observer. This period coincides with the period of the planet. Similar to the transit method, the RV method comes with observational bias. Like the transit method, the RV method is sensitive to short period planets, as they orbit closer and have a greater gravitational pull on their star so they produce a larger signal. The RV method is also sensitive to more massive planets, as is needed to cause a detectable red or blue shift in the absorption lines. While the transit method can give us the radius of the planet (when the star's radius is also known), the RV method gives us a measure of the planet's mass, if the host star mass is also known. These two features can lead us to the density profile of the planet and when used together allow us to gain major insight on planet populations.

To date, there have been no circumbinary planets discovered by the radial velocity method. Searches have occurred (Konacki 2005; Martin et al. 2019) but all have fallen short of identifying any new circumbinary planets. As mentioned prior, the RV method has a weaker bias towards short period planets than the transit method does, so they may be a better tool for identifying multi-planet systems as they could identify longer period planets. Additionally, the RV method has a shallower bias for edge on systems, which could help us find new systems that would go undetected by the transit method. For this reason, the RV method is still relevant and useful for the future of circumbinary planet studies.

1.1.3. *Circumbinary Planets*

When it comes to planets involved with binary star systems, there are two types of orbits, s-type and p-type, as shown in Figure 3. S-types orbit around the center of mass of one of the stars in the binary, also known as a circumprimary or circumsecondary planet. P-types orbit around the center

of mass of both the stars in the binary, also known as a circumbinary planet (CBP), which are the sole focus of this paper.

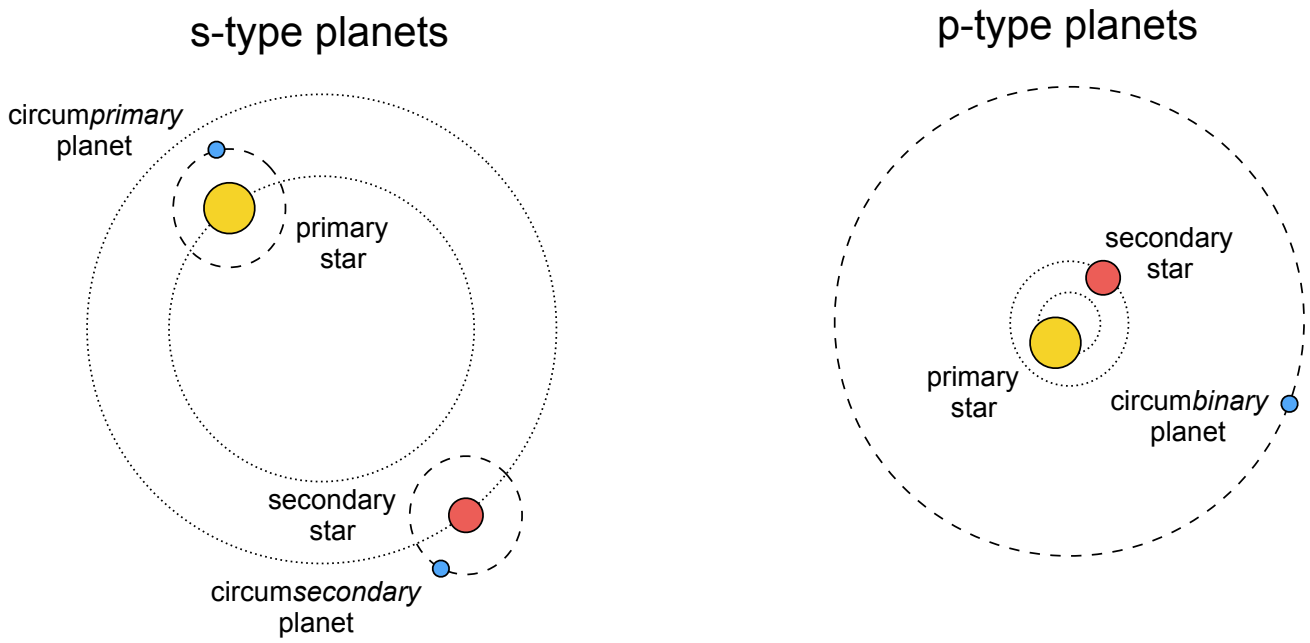

Figure 3. Left: S-type orbits where the planet orbits around the center of mass of only one of the stars in the binary. Right: P-type orbits where the planet orbits around the center of mass of both stars in the binary. These are the main focus of our study. Credit: Martin 2018.

There are currently 11 known transiting CBPs in 13 systems (Martin 2018; Kostov et al. 2020), including the three-planet Kepler-47 system (Orosz et al. 2019). Finding CBPs via the transit method is more complex than it is for planets around single stars because these planets can have variations in their transit times on the order of days, making automated detection methods for planets around single stars unusable. We are left with having to identify circumbinary planets by eye or develop new techniques (Windemuth et al. 2019; Martin and Fabrycky 2021). In addition, a typical lightcurve for a CBP like Kepler-16b will have not only the planet transits but also dips in light caused by the eclipse of the binary which could cover up a planet transit if they occur at the same time. The top image of Figure 4 shows the generic form of a lightcurve of an eclipsing binary. The bottom of Figure 4 shows the lightcurve of Kepler-16, an eclipsing binary, where the blue and yellow dips are

the primary and secondary eclipses, and the small green and red dips show the transits of each star by the circumbinary planet Kepler-16b.

While we may not be able to observe a clear transit, the gravitational pull of the planet can sometimes have an affect on the periodicity of the binary eclipse. If we observe what are known as eclipse-timing variations (ETVs), we may be able to infer the presence of a planet without seeing a direct transit. These ETVs also allow us to set an upper limit on the mass of this third body, which helps us establish that it is a planet and not another object like a tertiary star. The Kepler mission has been the most successful in finding CBPs so far, identifying 12 CBPs in 10 systems. However, most of the Kepler CBPs are found around distant stars, which makes follow up observations difficult. The TESS mission is expected to find more CBPs. It has already found one in TOI-1338. CBPs identified by TESS will be more useful for follow up observations as TESS is designed to look at the closest, brightest stars. Table 1 lists the name, binary parameters, and planetary parameters for all currently known CBPs. CBPs are a fantastic probe for furthering our understanding of the planetary life cycle as we can compare them against planets around single stars.

1.2. *Three Body Stability*

Understanding the mechanics for individual planets around single stars is generally trivial as the 2-body problem has a closed solution. When we expand up to the 3- and N-body problems, the mathematics complicates understanding as there is no closed form solution to rely on. Our method for simulating these N-body problems will be addressed in Section 2.1. In the case of circumbinary planets we use at minimum the 3-body problem. A number of different interactions can cause a disruption of stability for the orbits of our planets. A stable orbit is loosely defined as one that does not result in a collision between bodies or an ejection, but orbits evolve and a stable orbit at one point in time may turn into an unstable orbit later on due to the chaotic interactions in 3+ body cases. These interactions can come in different prescriptions like binary-planet and planet-planet interactions when the gravitational forces of each body have an influence on the behavior of the other bodies. Even the gravitational relationship between the stars in the binary can create "islands" of stability and instability for the planet throughout the disc. Examples of these islands

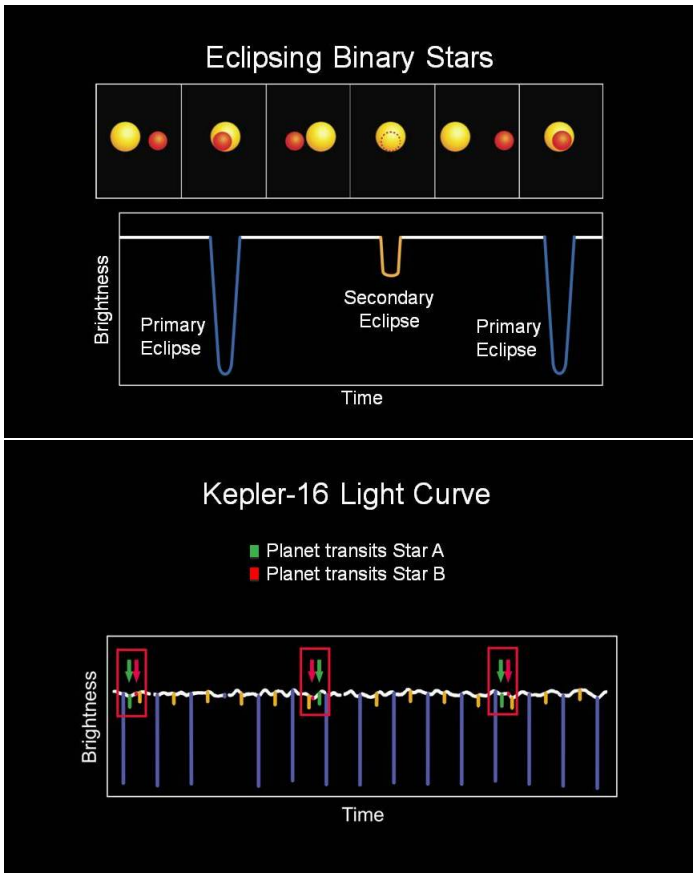

Figure 4. Top: A generic lightcurve for an eclipsing binary. Bottom: Lightcurve for Kepler-16 including features of the eclipsing binary and the transits of its circumbinary planet, Kepler-16b. Credit: NASA/JPL.

are shown in Figure 5. Green dots on the top graphs of Figure 5 show the position of the currently known planet, and there is ample stable space exterior to this position, so outer planets could be there.

1.3. *Mean Motion Resonances*

In the most simple context, resonance occurs when the ratio between planet periods has an integer value. In Figure 6, we see a stable configuration of a 2:1 resonance where the bodies start on the same side of their orbit with respect to one another, but they are separated. The resonance keeps the bodies from ever having an interaction in their orbits that could have negative consequences. In Figure 7, these bodies are yet again in a 2:1 resonance, but they start close to one another, and reach this position once every orbit causing a negative gravitational interaction that will result in

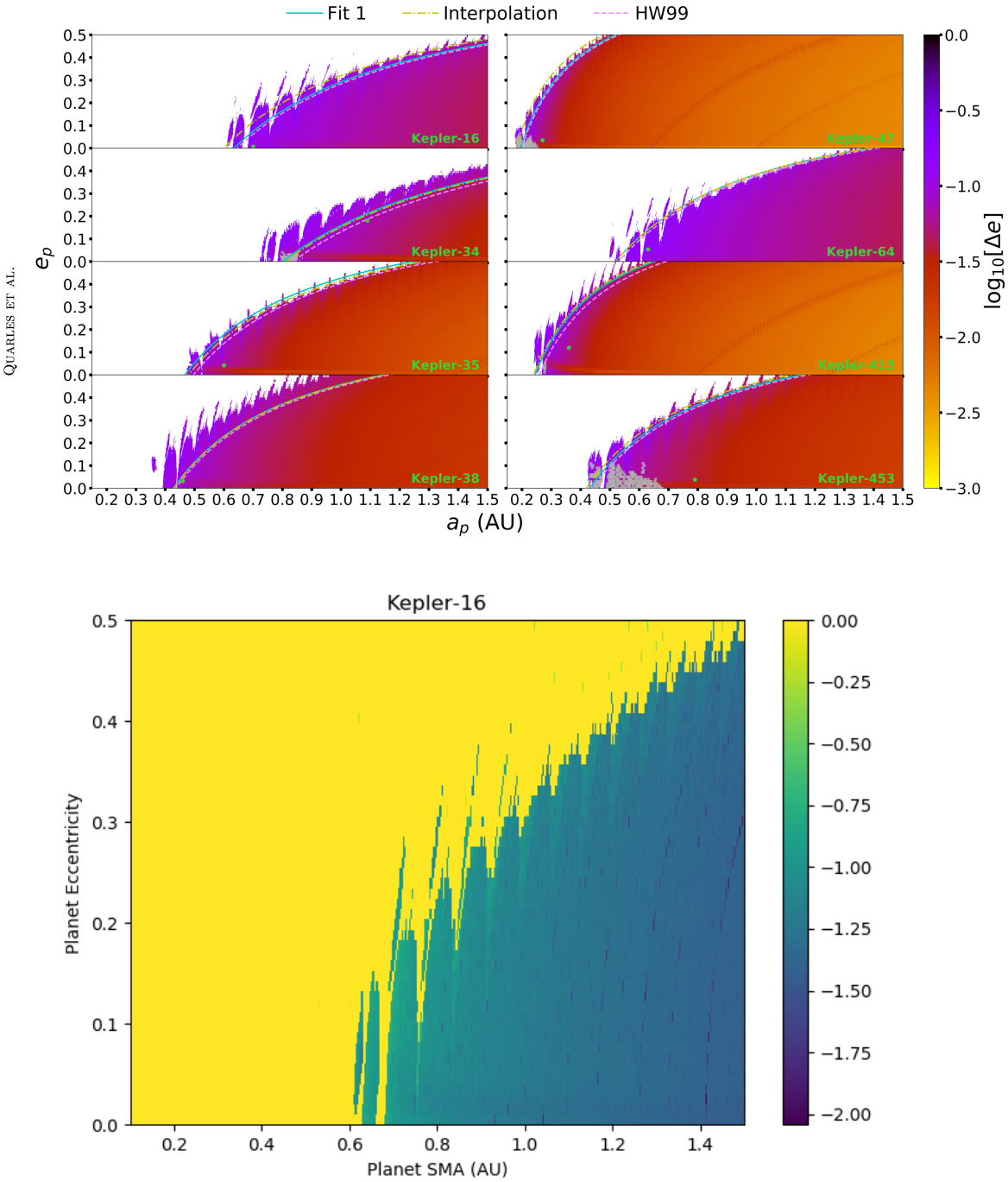

Figure 5. Top: Stability graphs from Quarles et al. 2018. White zones signify unstable regions, where the colorful 'islands' signify locations where a planet would be stable at a given eccentricity. The color scale indicates the maximum variation in eccentricity over a 100,000 year integration, using a log scale. Bottom: Our simple replication of the Quarles plot for Kepler-16, constructed using REBOUND. Yellow regions are unstable zones, while the purple and blue regions are stable 'islands' where the planet could be stable for an intersecting eccentricity and semi-major axis in those regions.

instability. Resonances play a major role in preserving or disrupting stability in multi-body systems. For example, the orbits of Neptune and Pluto cross one another, but they sit in a 3:2 resonance. This resonance is the reason that these bodies will never collide despite having crossing orbits, as they will never get near each other in their orbit.

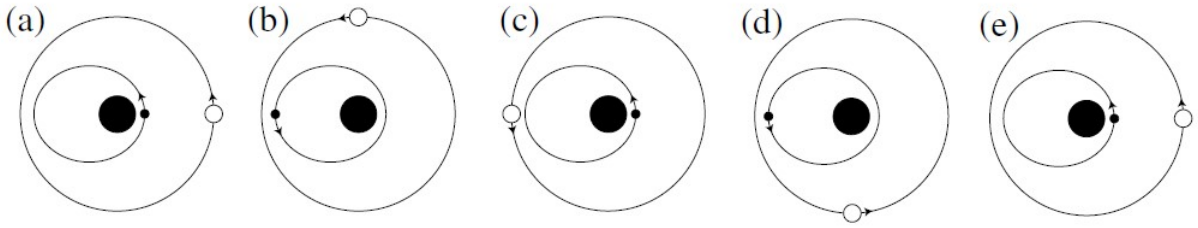

Figure 6. Relative positions of two bodies in a stable 2:1 resonant orbital configuration. Credit: *Solar System Dynamics*, Murray & Dermott

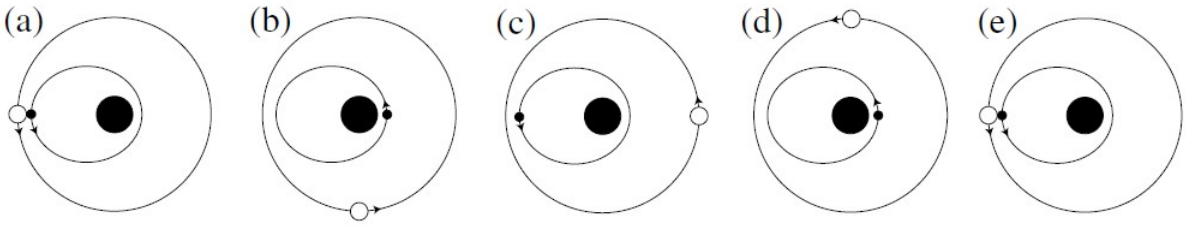

Figure 7. Relative positions of two bodies in an unstable 2:1 resonant orbital configuration. Credit: *Solar System Dynamics*, Murray & Dermott

Now we look at resonances in a more analytical sense, where the ratio of two orbital periods for bodies in the same system is given by:

$$\frac{P_{\rm o}}{P_{\rm i}} = \frac{n_{\rm i}}{n_{\rm o}} = \frac{p+q}{q}, \tag{1}$$

where we define $n = 2\pi/P$ as the mean motion of the orbit, and p and q are integers. Variables with the subscript 'o' represent that value for the outer body, while those with the subscript 'i', represent that value for the inner body. By convention, q is the order and p is the degree of the resonance. For example, a 2 to 1 resonance (commonly denoted as 2:1) is a first order, first degree resonance.

An integer ratio of periods may seem arbitrary, but a physical effect actually occurs. By definition, a resonance is present when one of the resonant arguments of the orbit librates around a fixed value, as opposed to circulating through a full range of 360°. This libration indicates that the orbits may exchange energy and angular momentum over long periods of time, and thus gravitational interactions will be amplified. In the case of a coplanar orbit, the resonant argument is defined by the following:

$$\phi = j_1\lambda_{\rm o} + j_2\lambda_{\rm i} + j_3\varpi_{\rm o} + j_4\varpi_{\rm i}, \tag{2}$$

where λ is the mean longitude, ϖ is the longitude of periapse and the j coefficients are integers that follow the d'Alembert relation,

$$\sum_{i=1}^{4} j_i = 0. \tag{3}$$

(Murray & Dermott 2000). For example, for a 2:1 resonance, the resonant arguments are:

$$\phi_1 = 2\lambda_{\rm o} - 1\lambda_{\rm i} - 1\varpi_{\rm o} \tag{4}$$

$$\phi_2 = 2\lambda_{\rm o} - 1\lambda_{\rm i} - 1\varpi_{\rm i} \tag{5}$$

For a mean motion resonance $j_1 = p + q$ and $j_2 = -p$, and then j_3 and j_4 are chosen to satisfy Eq. 3. A given resonance will have $q + 1$ resonant arguments. To be in resonance, only one of these resonant arguments must librate. Libration of one of the resonant arguments is shown in the top panel of Figure 8, where ϕ_1 is circulating the entire time, while ϕ_2 circulates, but librates from 10,000 to almost 40,000 years. The libration time corresponds to the time while the planets are in a 2:1 resonance on the period graph in the bottom panel of Figure 8. An interesting phenomenon in planet demographics has been the higher number of planets found just inside and outside of resonance values in their orbits.

We see around single stars that there are some planets in or at least near resonance. Figure 9 shows this phenomenon where there are peaks just outside of resonances like the 3:2 and 2:1. This is significant because of the difference in formation theory between planets around single stars and those around binaries. While there are restrictions on where planets can form around single stars, in situ

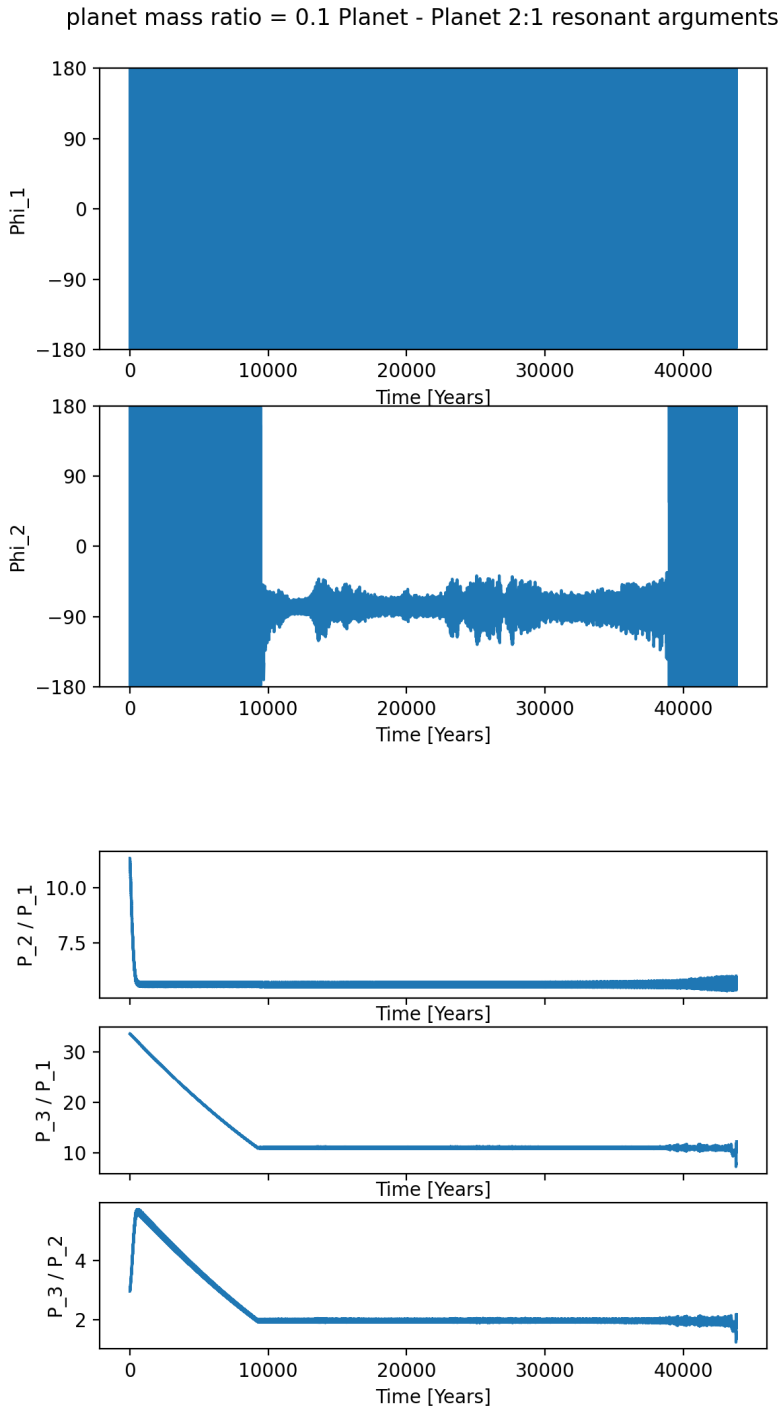

Figure 8. A migrating two-planet circumbinary system that starts out of resonance but migrates into and locks at a 2:1 resonance. Top: resonant angles (Eqs. 4 and 5) for a 2:1 planet-planet resonance. The angle ϕ_1 is quickly moving through a 360 degree cycle. Angle ϕ_2 begins librating shortly before 10,000 years, when the planets reach a 2:1 resonance. Shortly before 40,000 years the system leaves resonance and goes unstable. Bottom: period ratios with the binary (P_1), inner planet (P_2) and outer planet (P_3).

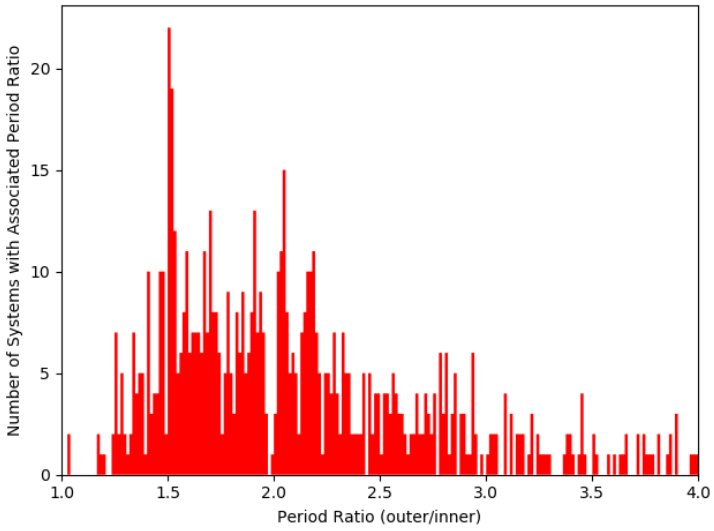

Figure 9. Histogram of period ratios for all multi-planet, transiting exoplanet systems in the NASA Exoplanet Archive.

formation in general is much more likely. This affect is likely what gives rise to these near resonance peaks as planets can form and stay there through their lifetime. Migration and resonant chains are not fully understood for single star situations, but they are thought to play a role for systems like Trappist-1. Stochastic forcing (Section 2.3) (Rein 2010) is a proposed method for disrupting resonances in these systems that migrate, and will be a featured part of our study. For binaries, we do not expect in situ formation, but rather migration to observed positions, and resonances are a natural byproduct of migration. We anticipate that multi-planet circumbinary systems are likely to be in resonant chains due to their history of migration. When looking at circumbinary planets, we consider resonances between the planet and the binary periods, as well as between the planet periods in multi-planet architectures. None of the currently known CBPs are in resonance with their binary, and the only known multi-planet CBP system, Kepler-47, does not possess any planet-planet resonances.

Given that in situ planet formation is disfavored for circumbinary planets (see later section), and migration will behave differently in a circumbinary disc we would not necessarily expect the same histogram for circumbinary planets.

1.4. *Circumbinary Discs*

Much like around single stars, binary stars can have discs of residual materials left over from their formation. These discs are what lead to planetary formation. We will look at how the disc interacts with the binary and planets formed farther out from the star to see how the interaction affects the final positions and stability of these planets.

The most notable interaction comes between the binary and the disc. These tidal interactions create an inner truncation of the disc where conditions are incredibly turbulent. This truncation exists around single stars, but for binaries it is much wider, sitting at roughly 2.5 times the separation of the binary, although the binary eccentricity impacts this positioning (Artymowicz & Lubow 1994).

The disc and planets will also pull and tug on one another. This interaction can cause migration, which is a notable feature that needs to be included when modeling these systems. The nature of migration is explored in Section 1.5.

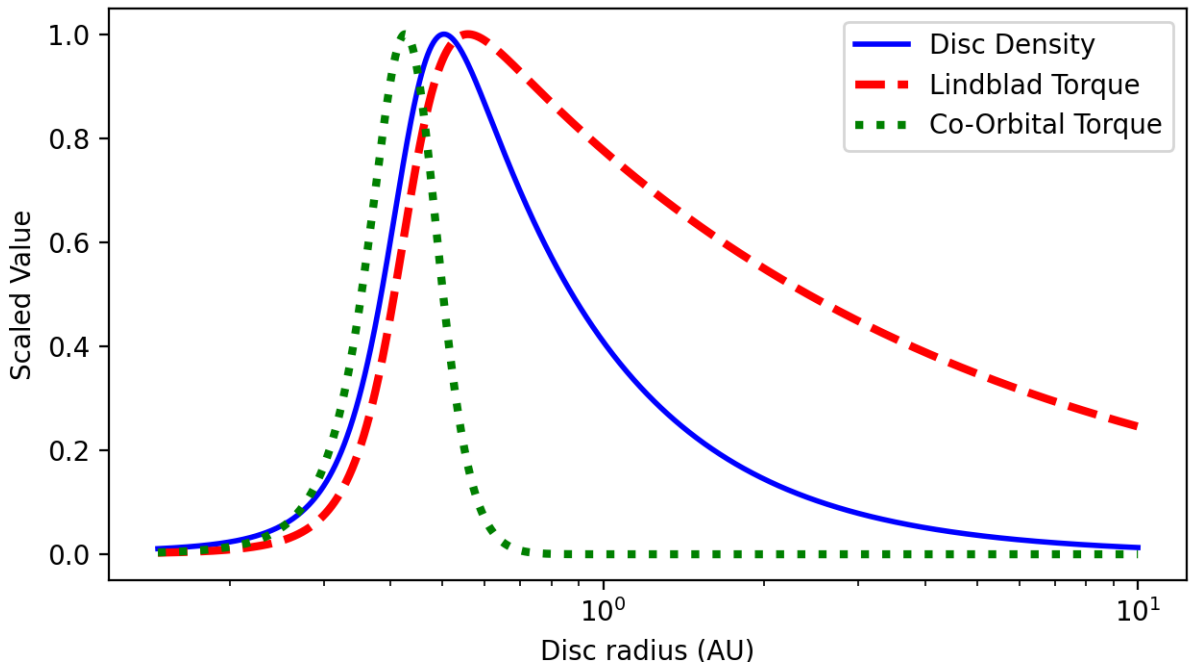

Figure 10. Example disc profile showing density, Lindblad torque, and Co-Orbital torque as they scale with respect to radial position in the disc

Figure 10 shows an example of a generic disc density profile and accompanying torques that will be present. More on this in Section 2.2

1.5. *Planetary Migration*

When a planet is present at the same time as the disc, they will interact with one another. Through this interaction, planets can be pushed closer to or farther from their host star(s). This process is known as migration and was theorized (Goldreich & Tremaine 1979) before the discovery of the first exoplanet. Many of the known CBPs have been observed close to their stability limit, which is defined by the parameters of the binary. In situ planet formation at these positions is thought to be highly unlikely (Bromley & Kenyon 2015), and so it is preferred that these CBPs form farther away from the binary and migrate into their observed positions (Pierens & Nelson 2013).

The mechanisms for this migration come in two different forms. Known as the Lindblad torque and co-orbital torque, the most simple description tells that the Lindblad torque forces planets closer in to the stars while co-orbital torques push them away. The stopping position of the planet will come where these two different torques balance. The following two subsections will look at a deeper description of these torques.

1.5.1. *Lindblad Torque*

As aforementioned, the Lindblad torque, simply put, causes inwards migration of the planet. The origin of this movement comes from the presence of Lindblad resonances. As the planet moves through the disk it exerts spiral density waves through the disk which bounce off of Lindblad resonances and come back to interact with the planet again. The outwards waves exert a stronger torque than that of the inwards waves, causing the planet to lose angular momentum and fall in towards the star. The strength of the torque depends on several factors, as shown in the following equation (Lubow & Ida 2010):

$$T_{Lind} = -\Sigma\ \Omega_p^2\ r^4\ \left(\frac{M_p}{M_s}\right)^2\ \left(\frac{1}{h}\right)^2 \tag{6}$$

$$\Omega\left(r\right) = \sqrt{\frac{GM_s}{r^3}} \tag{7}$$

where Σ is the surface density of the disc (dependent on the radial position and disc profile; see Eq. 10), r is the distance of the planet approximated as the semi-major axis, M_p and M_s are the masses of the planet and star respectively, and h is the scale height of the disk. Ω_p is the Keplarian orbital frequency of the planet as shown in Eq. 7.

1.5.2. *Co-orbital Torque*

Co-orbital or co-rotation torques generally cause outward migration of the planet. This comes from interaction between the gas directly in front of and behind the planet as it orbits. In the reference frame of the planet, this gas moves in a horseshoe shape. In front of the planet, the gas moves from further out in the disc to closer in, causing a buildup of cooler, denser gas. This density gradient between the gas in front of and behind the planet causes the planet to gain angular momentum and migrate outwards. The following equation describes the factors that define the value of the co-orbital torque (Lubow & Ida 2010):

$$T_{Co} = \Sigma\ \Omega_p^2\ r\ w^3\ \left(\frac{\Delta\Sigma}{\Sigma} - \frac{\Delta B}{B}\right) \tag{8}$$

$$R_{Hill} = r\ \left(\frac{M_p}{3\ M_s}\right)^{\frac{1}{3}} \tag{9}$$

where w is the width of the co-orbital horseshoe region, approximated to be equal to the Hill radius given in Eq. 9. Also, $\Delta\Sigma = \Sigma_o - \Sigma_i$, which is the difference in disk density between the outside and inside of the horseshoe region, and $\Delta B = B_o - B_i$, which is the value of B at the outer and inner edges of the horseshoe region, where $B = \Omega(r)/4$.

2. METHODS

In order to learn more about how the presence of multiple planets affects the migration and final positioning of these systems we run suites of numerical simulations with varying starting parameters. Section 2.1 explains the N-body simulator we implored. Section 2.2 touches on how we modeled migration, followed by Section 2.3 on an implemented feature known as stochastic forcing.

2.1. *N-body simulations*

We used the REBOUNDx (Tamayo et al. 2020) N-body code as the baseline for our numerical simulations. This code allowed us to easily create conditions with parameters to match known and artificially created binaries. We add in planets with parameters equal or similar to known CBPs. The program takes our input initial conditions like mass, semi-major axis, and eccentricity to calculate current conditions like velocity and position based on gravitational interactions of the present bodies. The code tracks the evolution of the conditions of the system which can offer us insight into how these systems evolve, like if planets get ejected or fall into stable orbits in resonance with the binary or other planets.

2.2. *Modeling Migration*

As mentioned in Section 1.4, planetary migration is a fundamental piece of this puzzle. In order to most accurately determine how our system evolves, we are tasked with correctly integrating a disc profile based on a simple prescription of what is used in more advanced hydrodynamical simulations. We base our disc off of the model used in Pierens & Nelson (2013). The fundamental piece is the definition of the disc surface density, $\Sigma(R)$ given by the following:

$$\Sigma(R) = f_{gap}\Sigma_o R^{-3/2} \tag{10}$$

$$f_{gap} = \left(1 + exp\left(-\frac{R - R_{gap}}{0.1R_{gap}}\right)\right)^{-1} \tag{11}$$

where f_{gap} is an exponential used to model the inner edge of the disc that we determine by establishing the value of R_{gap} as 3 times the separation of the binary, Σ_o is our value for the disc density, and R is the position in the disc from the center of mass.

As shown in Figure 10 the density profile of the disc gradually rises until a viscosity build up region is reached to which the density drops off steeply and does not recover. An important factor in our numerical simulations is that we do not vary the existence of the disc, meaning that the disc does not dissipate or accrete material, and thus is interacting during the entire timescale of migration that we simulate over. These timescales are reasonable compared to the lifetime of a disc. We define our disc by establishing variables that are needed to calculate the Lindlbad and co-rotation torques. The key difference between the Lindblad and co-rotation torques are their dependence on the parameters

of the disc. The Lindblad torque depends directly on the value of Σ_o, while the co-rotation torque depends on $d\Sigma/dr$, the differential of the disc density as a function of radial position. This difference is why the Lindblad torque dominates through most of the disc causing inward migration, while near the inner edge of the disc where there is a density buildup, the differential raises and the co-rotation torque grows stronger and acts in opposite to the Lindblad torque. The equalization of these torques is the foundation for stopping planets at this position. From Pierens & Nelson (2013), we define the stability limit for the disc, to generally be 2.5-3 times the value of the separation of the binary.

We utilize the functionality of REBOUNDx (Tamayo et al. 2020) to add migration to our simulations. Migration is modeled by calculating the Lindblad and co-rotation torques at each time step, and continuing to move the planet in or out at speeds determined by the proportion of these values to one another. The stopping location for the inner planet comes when these two values are equal, which is generally very near or at the stability limit. We can see this in a generic form in Figure 10, where the stopping position is located by the crossing point of the red-dashed and green-dotted lines, which are the Lindblad and co-orbital torques respectively. We artificially balance the peaks of the torques to be equal, which is generally not the case based on the mathematics. The inner planet will be made to stop where the known planet is observed. We are confident in this scaling because the underlying assumption is that planets do stop at the disc inner edge. We utilize this assumption to probe what happens when this stopping occurs and other planets are present. We do not incrementally add in new planets when modeling multi-planet systems, but rather start them at separations outside of resonances to allow them to migrate in, potentially hit and stick into resonance, or to cause chaotic reactions that result in ejection.

2.3. *Stochastic Forcing*

Stochastic forcing is a method for modeling turbulence in a disc (Rein 2010). This turbulence can cause disruption in resonant chains, possibly contributing to non-resonant features in the histogram in Figure 9. We believe stochastic forcing to be applicable to our simulations due to the high level of turbulence caused by the binary near the disc edge, where most of our single planet systems are found near. Figure 11 shows a model from Kley et al. (2019) that shows a planet (blue-dashed line)

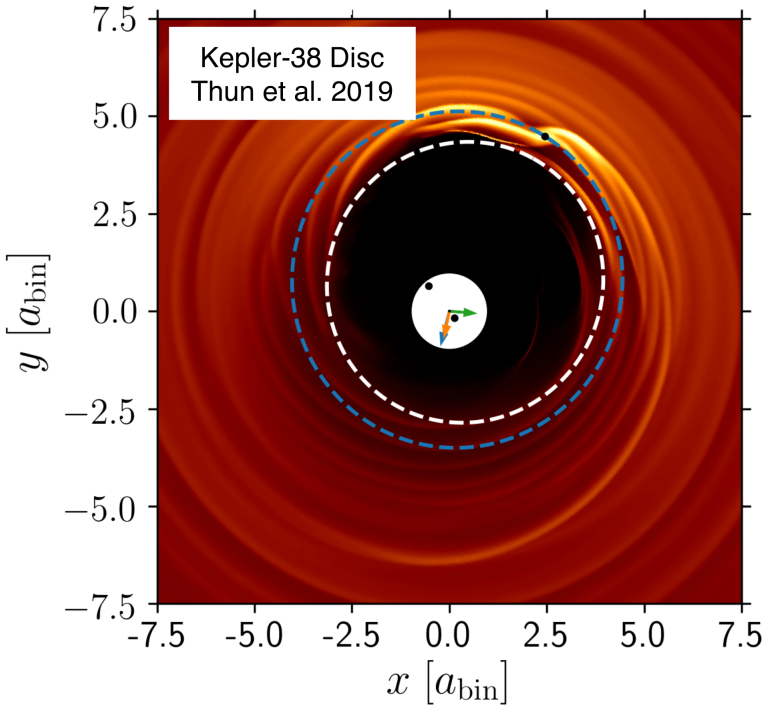

Figure 11. Hydrodynamical disc model representation for Kepler-38 showing the planetary orbit (blue-dashed circle) near the stability limit/disc inner edge (white-dashed circle).

near its stability limit (white-dashed line) and their hydrodynamical disc model showing the swells and swirls of the disc that cause this turbulence. Simply put by the name, stochastic forcing means to randomly apply a force in a random direction every so often. The timescale for this application comes on the order of the orbital period of the planet. The force values are calculated using the following equations:

$$F = F * exp\left(\frac{-dt}{\tau}\right) \tag{12}$$

$$F = F + \left(\alpha_{stoch}\ X_i \sqrt{1 - exp\left(\frac{-2\ dt}{\tau}\right)}\right) \tag{13}$$

where F is the value of the force, dt is the change in time from the previous step, τ is the timescale of application set to roughly 5 times the orbital period of the binary (since this will be roughly the orbital period of a planet near the stability limit), and X_i is a randomly generated scaling factor from a normal distribution with mean equal to 0 and standard deviation equal to 1. The parameter

α_{stoch} is determined by the following:

$$\alpha_{stoch} = \alpha * a_{central} \tag{14}$$

where α is a free parameter that we set to somewhere on the order of 10^{-6} to 10^{-4}, while $a_{central}$ is the gravitational acceleration due to the central stars. This force is independently calculated and applied to both the x and y components of the planet. Our simulations only apply this forcing to the innermost planet, and in case of an ejection, if the outer planet becomes the only planet in the system, the forcing begins to be applied to it.

3. RESULTS

The table below displays the parameters we used to recreate the known CBP systems in order to add new outer planets. All data comes from the NASA Exoplanet Archive.

Binary and Planetary Parameter Set

Planet Name	M_a	M_b	a_{bin}	e_{bin}	P_{bin}	m_p	$a_{p,obs}$	P_p	e_p
Kepler-16 b	0.6897	0.20255	0.22431	0.15944	46.7332	0.33	0.7048	228.776	0.0069
Kepler-34 b	1.0479	1.0208	0.22882	0.52087	39.06287	0.22	1.0896	288.822	0.182
Kepler-35 b	0.8877	0.8094	0.17617	0.1421	28.67134	0.127	0.60347	131.458	0.042
Kepler-38 b	0.949	0.249	0.1469	0.1032	21.11459	0.384	0.4632	105.59	0.032
Kepler-47 b	0.957	0.342	0.08145	0.0288	8.680882	0.006513	0.2877	49.4643	0.021
Kepler-64 b	1.528	0.408	0.1744	0.2117	21.5249	0.531	0.652	138.317	0.0702
Kepler-413 b	0.82	0.5423	0.10148	0.0365	13.04208	0.211	0.3553	66.262	0.1181
Kepler-453 b	0.944	0.1951	0.185319	0.0524	29.9969	0.050	0.7903	240.503	0.0359
Kepler-1661 b	0.841	0.262	0.187	0.112	32.21421	0.053	0.633	175.06	0.057
TOI-1338 b	1.038	0.2974	0.1288	0.15601	16.57518	0.104	0.4607	95.174	0.0880

where M_a and M_b are the primary and secondary star masses in stellar masses, a_{bin} is the binary separation in AU, e_{bin} is the binary eccentricity, P_{bin} is the binary period in days, m_p is the mass of the planet in Jupiter masses, $a_{p,obs}$ is the planet observed semi-major axis in AU, P_p is the planet period in days, and e_p is the planet's eccentricity.

3.1. *Recreation and Parameter Establishment*

In order to establish a baseline parameter set for aspects such as the disc density and scale height, we replicated a plot from Penzlin et al. (2021). The goal was to replicate the migration and stopping of these planets at their observed position. While starting semi-major axes for the targets may vary by tenths of a factor of the observed semi-major axis, most of the planets in our simulations migrate to their observed positions on roughly the same timescale, and all end up at their observed positions after a sufficient number of binary periods. Based off of this replication, our disc parameters are set at a disc density, $\Sigma_o = 70,000\ g/cm^3$ and a scale height, $h = 0.04$. These parameters are consistently used for all subsequent simulations unless otherwise explicitly stated. Experienced readers may note that this value for Σ_o is unusually high. The rate of migration for a planet of a given mass is linear with the value of Σ_o and in order to match with our N-body simulations what we see from hydrodynamical simulations like Penzlin et al. (2021), we scaled this value up by hand. We acknowledge that this value is too high to be physical but we required an empirical scaling factor due to the simplicity of our migration model equations which rely on many assumptions. These equations are also not calibrated for a binary but overall these issues should not influence the general trends produced in our simulations.

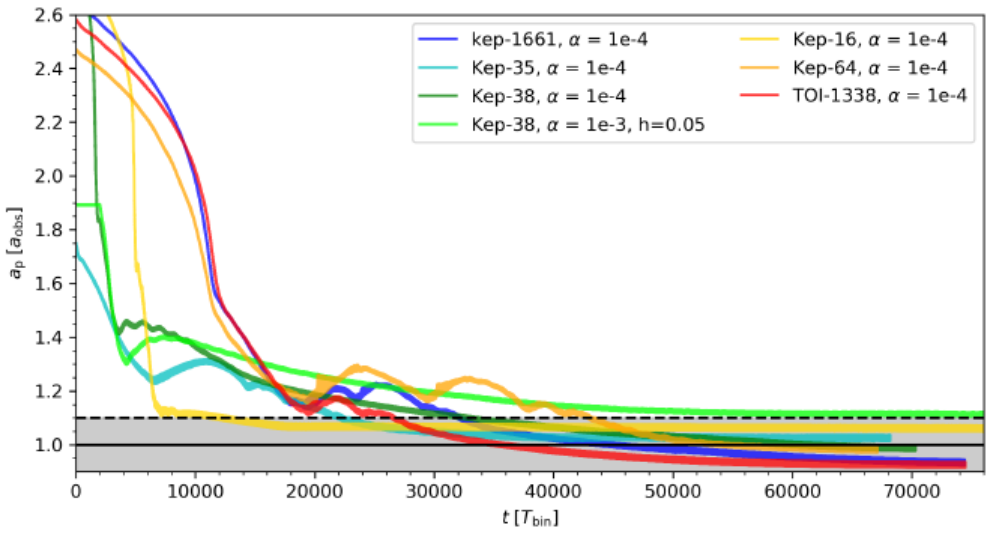

Figure 12. Plot from Penzlin et al. (2021) showing migration and parking of circumbinary planets to their observed positions using their hydrodynamical simulations

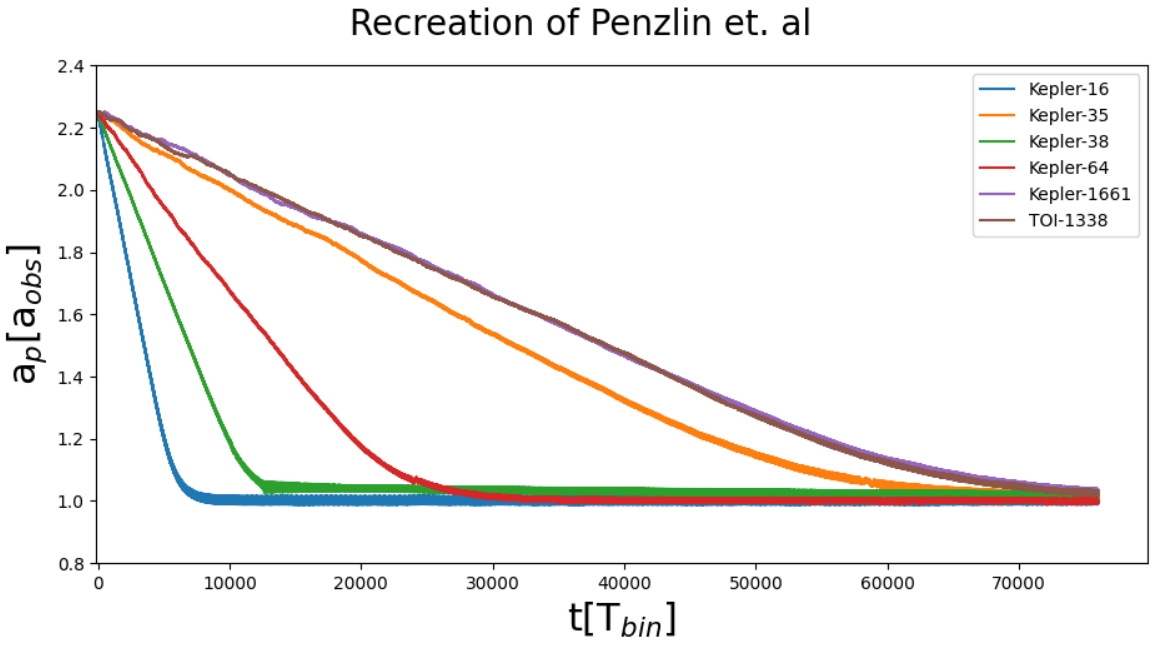

Figure 13. Our replication of the Penzlin figure using our N-body numerical simulations. The Penzlin curves have more wobble, but this is likely caused by a more complex disc model since they used a 2D hydrodynamical simulation. The final positions of the planets in the Penzlin figure are near the true stopping positions, while ours are dead on, due to the fact we tune our torques to stop the planet at its known position.

3.2. *Initial Simulations*

3.2.1. *Introduction*

We set up our simulations by feeding REBOUND the binary parameters, adding in a planet with parameters equal to those of the corresponding CBP of that system, and finally adding in an outer planet with a varying mass. We express the mass relationship as a ratio (given by q) of the outer planet mass to the inner planet mass as shown in Eq. 15.

$$q = \frac{m_{outer}}{m_{inner}} \tag{15}$$

Our initial simulations were ran over 150,000 years, long enough to see resonant locking if it were to occur, although this timescale is dependent on the migration timescale which depends on the density of the disc and the mass of the planets. Each simulation is started with its given binary parameters, with an inner planet equal to the mass of the known circumbinary planet in that system. For each simulation, the inner planet is started at a semi-major axis (SMA) that corresponds to roughly a 400 day period, while the outer planet is started at an SMA that corresponds to a period of roughly 1200 days. The simulations are ran with a varying outer planet mass, given by a ratio to the inner planet mass. We initially test the 0.1, 1, and 10 mass ratio cases to test the fate of the system. Stochastic forcing is enabled in these simulations, with $\alpha = 10^{-5}$ (similar to Rein 2010).

3.2.2. *Generic Features*

Figure 14 shows our simulation of Kepler-16 over 150,000 years. We can use it as a test case to analyze generic features that will be recurring in other systems throughout the Results section.

We start with the $q = 0.1$ mass ratio case (blue curves). In this situation, the inner planets line is covered by the other mass ratio regimes, but it follows the same general path. Each planet migrates inwards, with the ten times more massive inner planet doing so more quickly.

After 500 years the inner planet reaches its stopping point at the inner boundary of the disc which corresponds to a period of 230 days, which is the true period of Kepler-16b. The outer planet continues to migrate in until its reaches a 3:2 resonance after 1000 years, to which it stays locked in this orbital configuration until the end of our simulation.

The fate of the system for the $q = 1$ mass ratio regime differs. Since the inner planet is always a replication of the known planet for a given system, it follows the same natural path in each regime before the outer planet gets involved. The outer planet is more massive than in the $q = 0.1$ ratio case, so it migrates in faster. At 1000 years, the outer planet reaches the 2:1 resonance. Like for $q = 0.1$, there is a resonant locking. The difference here though is that in this case the outer planet has more angular momentum than the inner. This causes the outer planet to continue moving in, whereas it was stalled in the $q = 0.1$ case. This causes the inner planet, locked in the 2:1 resonance, to be forced closer to the binary. The result of this is an unstable interaction between the inner planet and the binary, causing its eccentricity to be pumped up above 1 and be ejected shortly after 1000 years. This ejection interacts with the outer planet, causing it to be pushed out slightly but not itself ejected. The outer planet then migrates inwards and parks at the same 230 day orbit where the now-ejected planet originally was.

For the $q = 10$ mass ratio case, the outer planet yet again migrates in on a shorter timescale. After 30 years, the outer planet pushes in the inner planet to the zone of instability, as was the case for $q = 1$. Interestingly, this planet is not ejected but is just pushed out to a wider orbit. The previously outer planet continues to migrate in and stop at the inner disc boundary. The previously inner planet, after surviving a near-ejection, migrates inwards again. At 800 years, the originally-inner planet locks into a resonance with the originally-outer planet, until eventually locking into a 2:1 resonance. With the planets having exchanged positions such that the heavier planet is now on the inside, this is conceptually similar to the $q = 0.1$ case. This has been coined the 'fountain effect' by Dan Fabrycky, and will occasionally be present in our simulations. One difference is seen though in comparison with the $q = 0.1$ case though that after a period of resonant locking this outer planet is ejected from the 2:1 resonance. Such an effect is likely due to the delicate inter-play between planet-planet and planet-binary resonances, which may sometimes work in concert to enhance a planet's eccentricity to the point of ejection, as was detailed in Sutherland & Kratter (2019).

Ejections of the inner planet, and occasionally both the inner and outer planet, can occur for all mass ratio regimes. An important result of our simulations is that resonant locking does not show

itself for mass ratio regimes greater than 1. We will delve deeper into the specifics of the full suite of our simulations to highlight the notable features that occur, and to define a transition region for when we see resonant locking versus ejection.

3.2.3. *Stable for a $q = 0.1$ Mass Ratio*

In our initial suite of simulations, Kepler-16, Kepler-35, and Kepler-64 were the only cases able to produce resonant locking in the $q = 0.1$ mass ratio regime as shown in Figures 14, 15, and 16 respectively. Kepler-16 shows a locking at the 2:1 resonance in this mass regime, while Kepler-35 appears to fall into a tighter resonance like the 4:3, and Kepler-64 exhibits a hangup at the 2:1 resonance before moving into the 4:3 resonance. In the $q = 1$ and $q = 10$ mass ratio regimes, all of the cases migrate inwards until the outer planet forces the inner planet inwards into the zone of instability, causing an elevation of the eccentricity and an ejection of the inner planet. In some cases, like Kepler-16 and Kepler-64, the outer planet continues to migrate in and stops at the inner edge of the disc where the inner planet was originally parked. Kepler-35 shows the case in the $q = 1$ regime where the outer planet interacts with the ejecting inner planet, and they both get ejected. The $q = 10$ case in Kepler-16 exhibits the aforementioned 'fountain' effect.

3.2.4. *Unstable for All Mass Ratios*

In the initial set of simulations, Kepler-34, -38, -413, -453, -47, -1661, and TOI-1338 were all unable to produce any resonant locking features that would last until the end of the simulations, shown in Figures 17, 18, 19, 20, 22, and 23. All mass ratio cases resulted in single or double planet ejections. Fountain effects can be seen in the $q = 10$ mass ratio regimes for Kepler-1661 and TOI-1338.

As mentioned in Section 3.3.1, we started all of our initial simulations with an inner planet period 400 days, and an outer planet period 1200 days. This was only a generic case and poses an issue with the migration timescale. We have noted a critical need for the inner planet to have reached its final parking position at the inner edge of the disc in order for the outer planet to move into a resonant locking situation. Since the inner boundary of the disc is dependent on the binary separation and eccentricity (Artymowicz & Lubow 1994), the final period of the inner planet is not always 400 days.

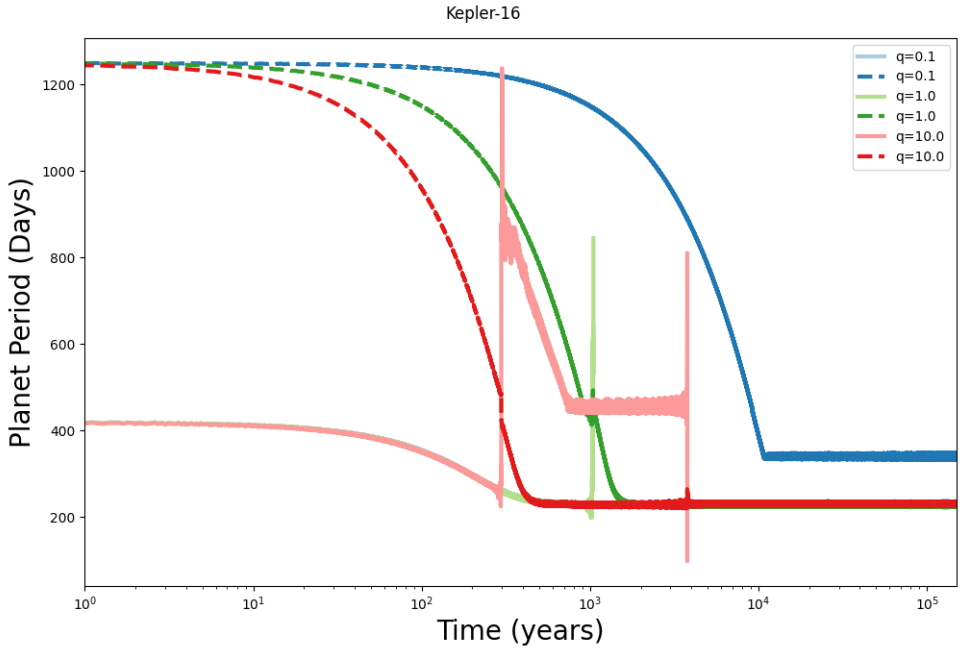

Figure 14. Initial simulation over 150,000 years showing the evolution of the planet periods for an inner planet with parameters equal to that of Kepler-16 b, and an outer planet of mass ratios $q = 0.1,\ 1$, and 10.

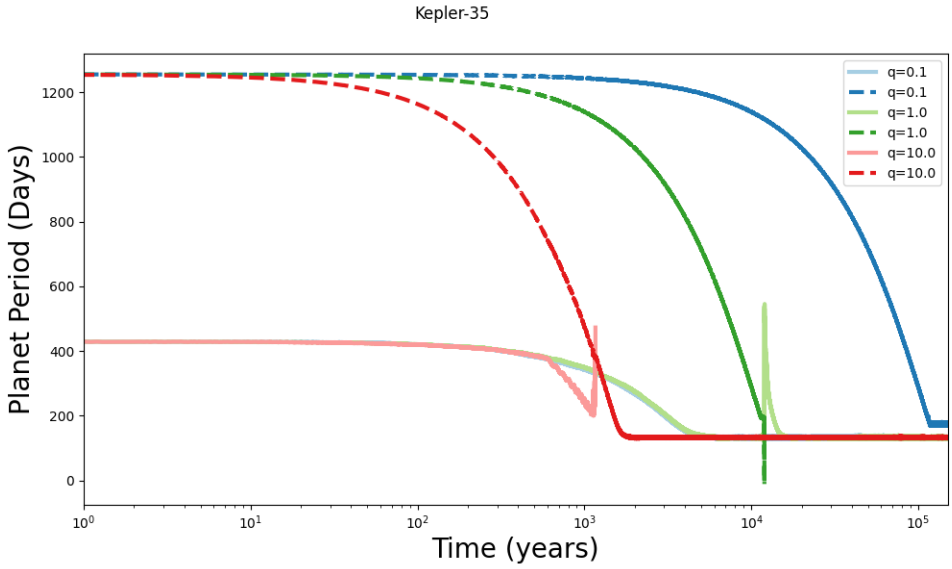

Figure 15. Initial simulation over 150,000 years showing the evolution of the planet periods for an inner planet with parameters equal to that of Kepler-35 b, and an outer planet of mass ratios $q = 0.1,\ 1$, and 10.

To allow for migration of the inner planet to reach its final position prior to an interaction with the

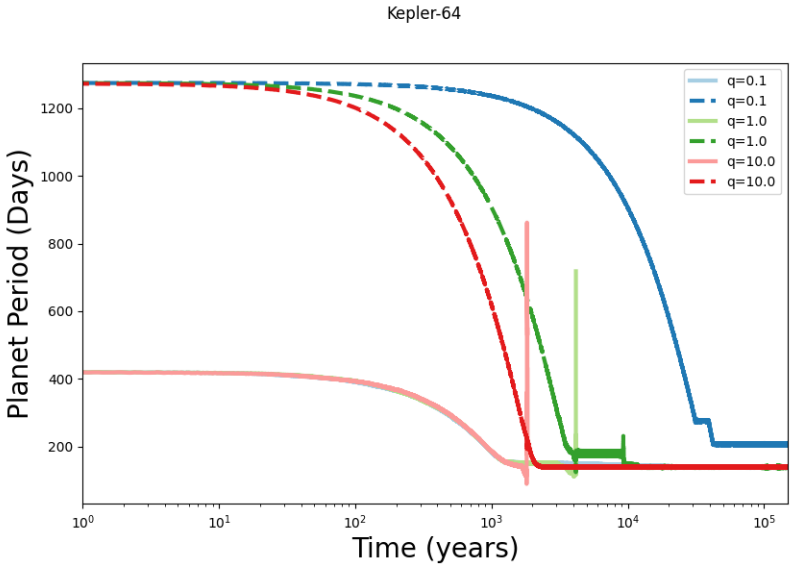

Figure 16. Initial simulation over 150,000 years showing the evolution of the planet periods for an inner planet with parameters equal to that of Kepler-64 b, and an outer planet of mass ratios $q = 0.1,\ 1$, and 10.

outer planet, we tuned each system to start at a position that would allow it do so, based on the known period of the inner planet. The next section covers this second sweep of simulations.

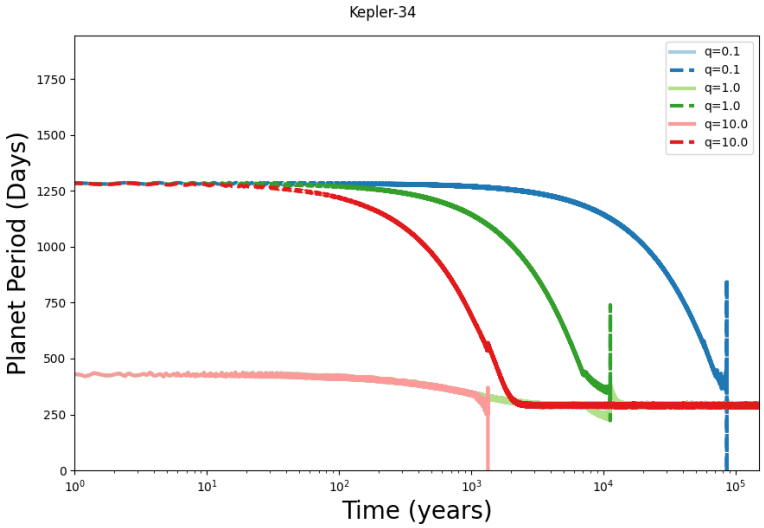

Figure 17. Initial simulation over 150,000 years showing the evolution of the planet periods for an inner planet with parameters equal to that of Kepler-34 b, and an outer planet of mass ratios $q = 0.1,\ 1$, and 10.

3.3. *Second-Round Simulations*

3.3.1. *New Parametrization*

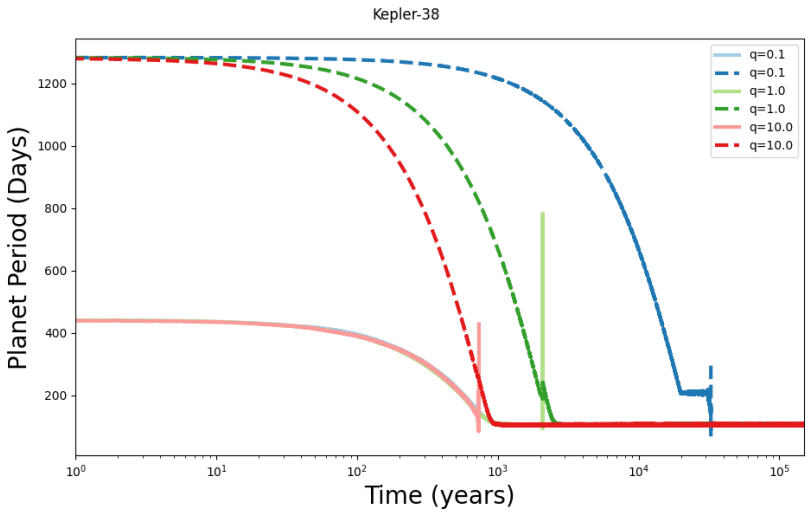

Figure 18. Initial simulation over 150,000 years showing the evolution of the planet periods for an inner planet with parameters equal to that of Kepler-38 b, and an outer planet of mass ratios $q = 0.1,\ 1$, and 10.

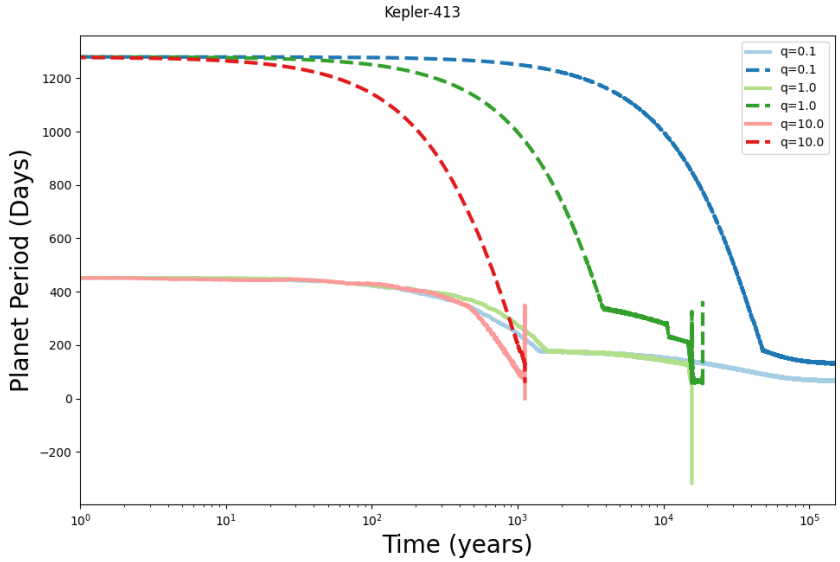

Figure 19. Initial simulation over 150,000 years showing the evolution of the planet periods for an inner planet with parameters equal to that of Kepler-413 b, and an outer planet of mass ratios $q = 0.1,\ 1$, and 10.

In this new sweep of simulations, we sharpen the starting positions of our inner and outer planets to allow the inner planet to reach its stopping position prior to interacting with the outer planet. These starting positions vary for each system and are dependent on the final period of the known

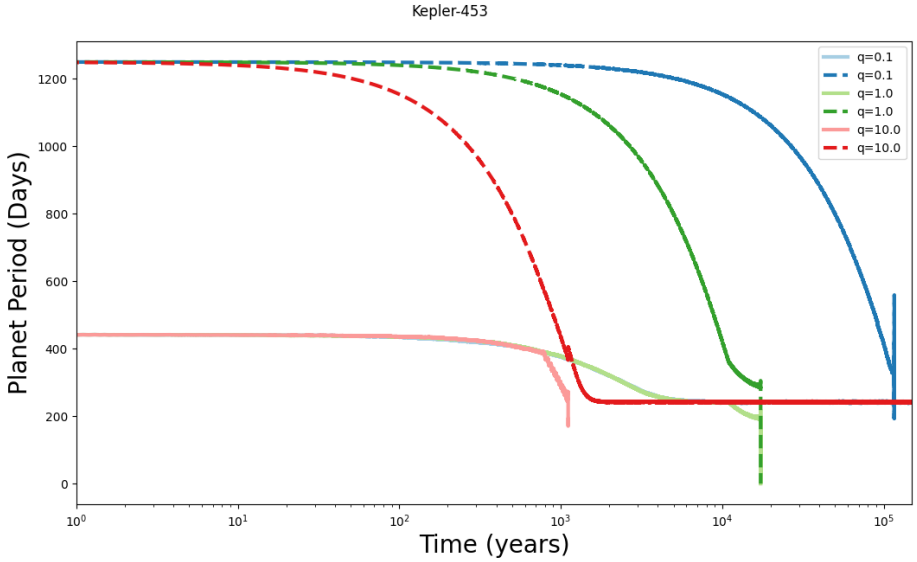

Figure 20. Initial simulation over 150,000 years showing the evolution of the planet periods for an inner planet with parameters equal to that of Kepler-453 b, and an outer planet of mass ratios $q = 0.1,\ 1$, and 10.

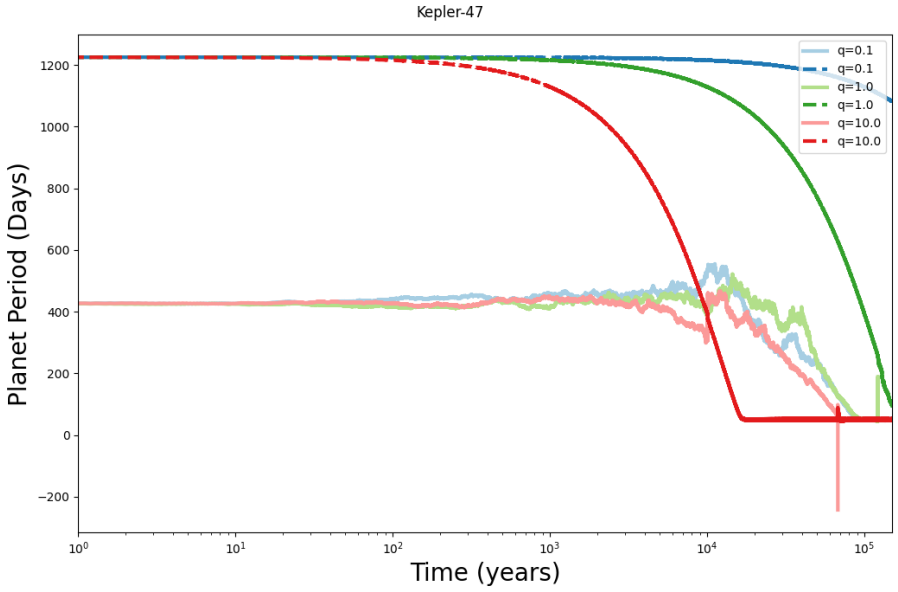

Figure 21. Initial simulation over 150,000 years showing the evolution of the planet periods for an inner planet with parameters equal to that of Kepler-47 b, and an outer planet of mass ratios $q = 0.1,\ 1$, and 10.

planet in the system. We subsequently move the outer planet to a position that is roughly 3 times the new starting period of the inner planet.

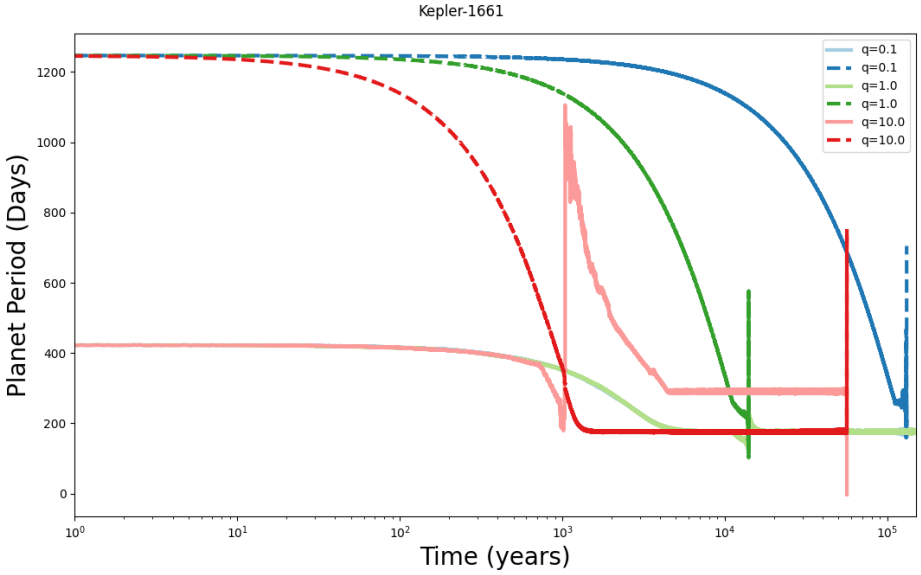

Figure 22. Initial simulation over 150,000 years showing the evolution of the planet periods for an inner planet with parameters equal to that of Kepler-1661 b, and an outer planet of mass ratios $q = 0.1,\ 1$, and 10.

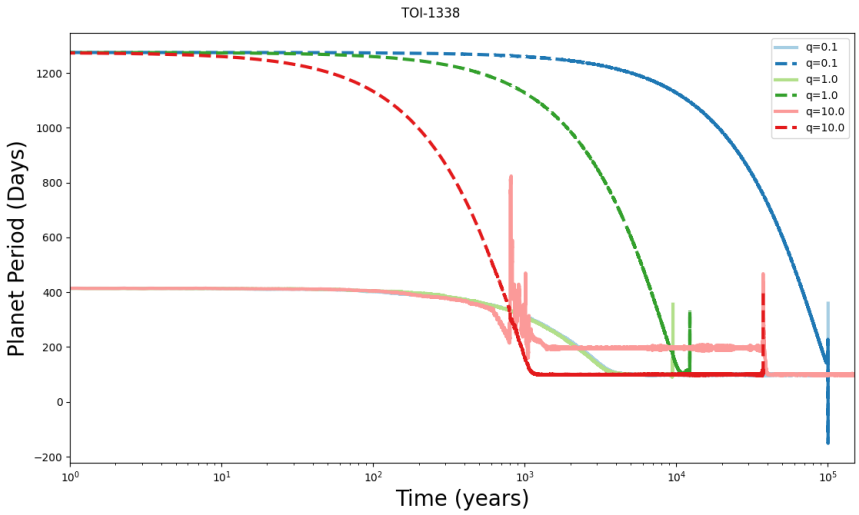

Figure 23. Initial simulation over 150,000 years showing the evolution of the planet periods for an inner planet with parameters equal to that of TOI-1338 b, and an outer planet of mass ratios $q = 0.1,\ 1$, and 10.

We zero in on a mass ratio case of $q = 0.05$. Figure 24 shows a replication of our initial simulation parameters with adjusted starting positions for TOI-1338. Resonant locking occurred but did not stick around until the end of our simulation for the $q = 0.1$ mass ratio case, which was consistent

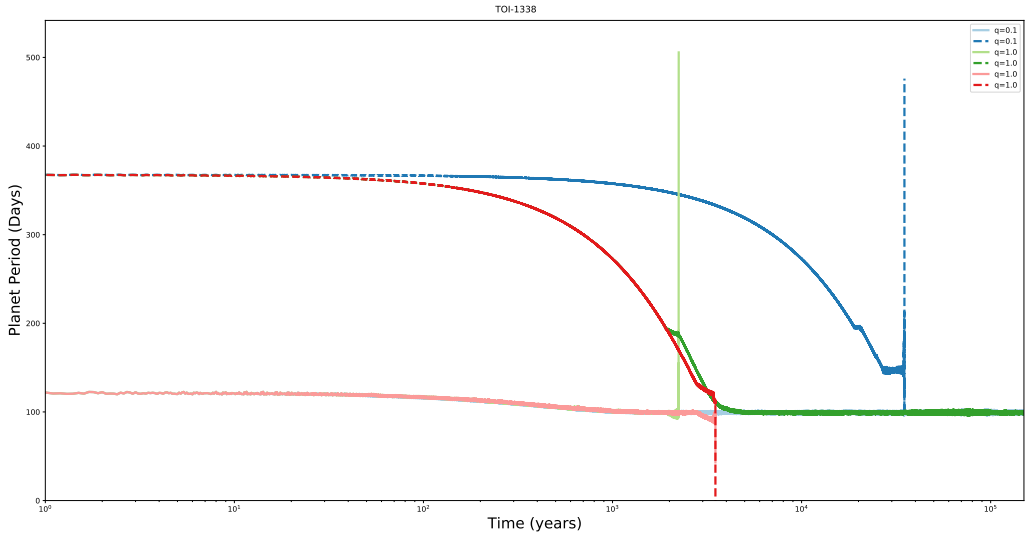

Figure 24. Second round simulation over 150,000 years after adjusting the starting positions of the inner and outer planet to allow the inner planet to migrate to its stopping position before interacting with the outer planet. Showcases an inner planet identical to TOI-1338 b, with an outer planet of varying mass ratio of $q = 0.1,\ 1$, and 10.

for all other systems when we adjusted the starting positions. This supports our decision to move to a lower mass ratio value, and we will double back on this decision as well in the following section. Another feature shown in Figure 24 is the effect of stochastic forcing on the behavior of the system. Unlike other figures, the $q = 1$ mass ratio is run twice with all parameters being the same. Stochastic forcing causes the time of ejection of the inner planet to change, as well as the fate of the outer planet. To analyze this effect, on top of moving to the $q = 0.05$ case, we also vary the value of the stochastic forcing parameter α by single orders of magnitude.

3.3.2. $\alpha = 10^{-5}$ *Case*

With our new mass ratio set to $q = 0.05$ and the starting positions for the inner and outer planets adjusted to allow for proper migration, we start with the stochastic forcing parameter α set to 10^{-5}. Kepler-38 was the only system where resonant locking was able to occur and be present at the end of the simulation, shown in Figure 25. It interestingly showed a hangup at the 2:1 resonance, followed by further migration into the 3:2 resonance. At this α value, all the other systems were unable to stay in resonance throughout the entire simulation.

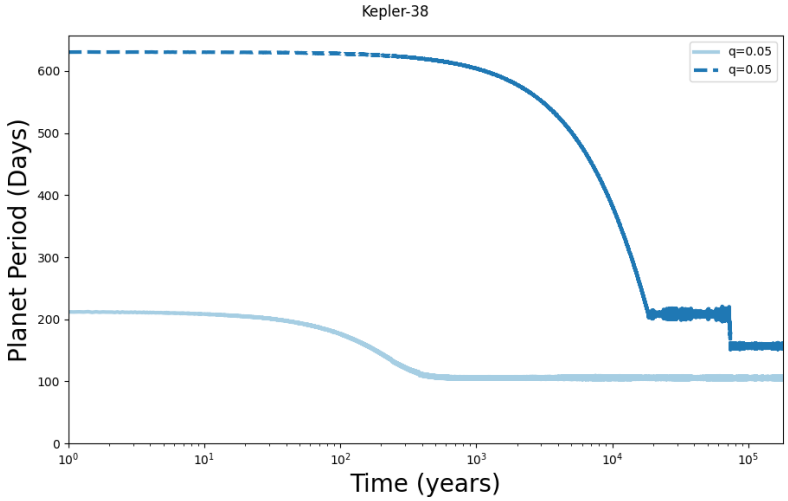

Figure 25. Second round simulation over 180,000 years after adjusting the starting positions of the inner and outer planet to allow the inner planet to migrate to its stopping position before interacting with the outer planet. Showcases an inner planet identical to Kepler-38 b, with an outer planet of mass ratio $q = 0.05$. Stochastic forcing parameter, α set to 10^{-5}.

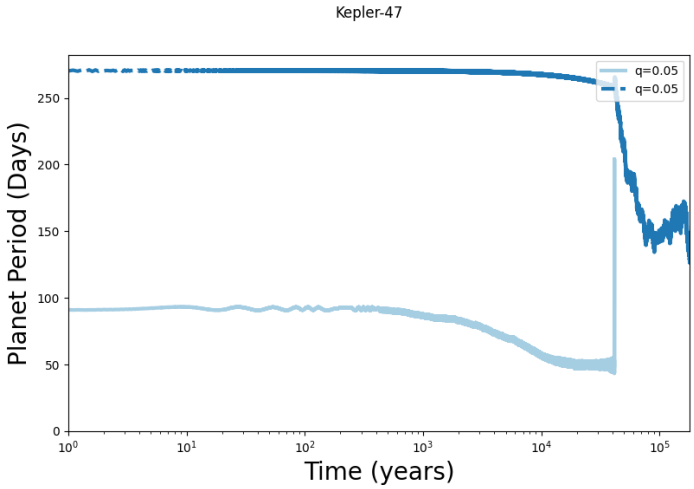

Figure 26. Second round simulation over 180,000 years after adjusting the starting positions of the inner and outer planet to allow the inner planet to migrate to its stopping position before interacting with the outer planet. Showcases an inner planet identical to Kepler-47 b, with an outer planet of mass ratio $q = 0.05$. Stochastic forcing parameter, α set to 10^{-5}.

3.3.3. $\alpha = 10^{-6}$ *Case*

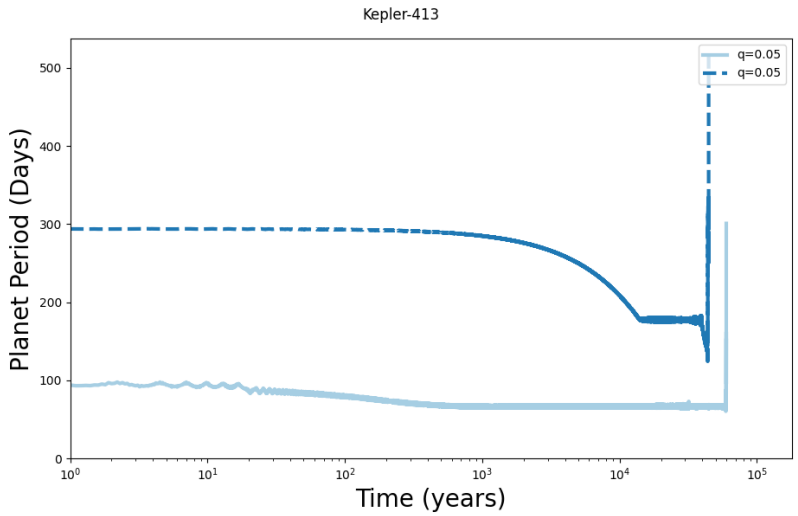

Figure 27. Second round simulation over 180,000 years after adjusting the starting positions of the inner and outer planet to allow the inner planet to migrate to its stopping position before interacting with the outer planet. Showcases an inner planet identical to Kepler-413 b, with an outer planet of mass ratio $q = 0.05$. Stochastic forcing parameter, α set to 10^{-5}.

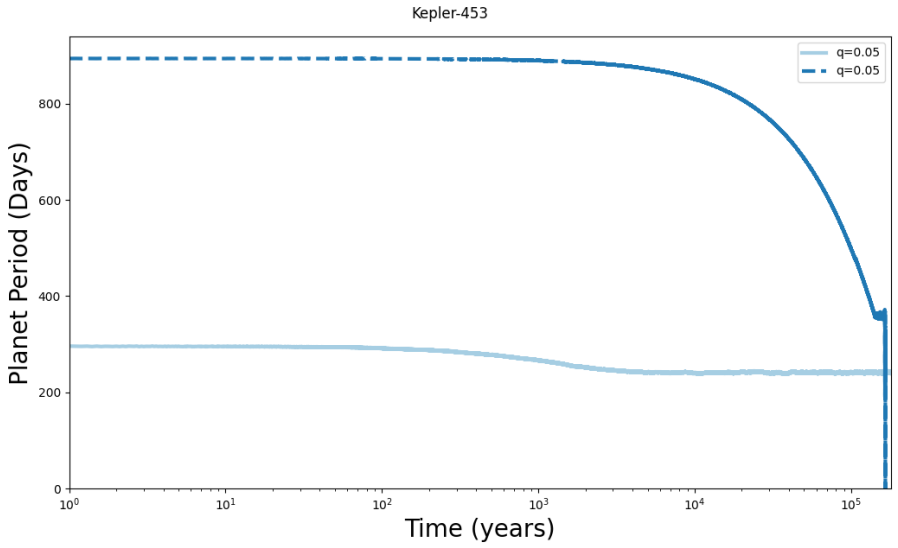

Figure 28. Second round simulation over 180,000 years after adjusting the starting positions of the inner and outer planet to allow the inner planet to migrate to its stopping position before interacting with the outer planet. Showcases an inner planet identical to Kepler-453 b, with an outer planet of mass ratio $q = 0.05$. Stochastic forcing parameter, α set to 10^{-5}.

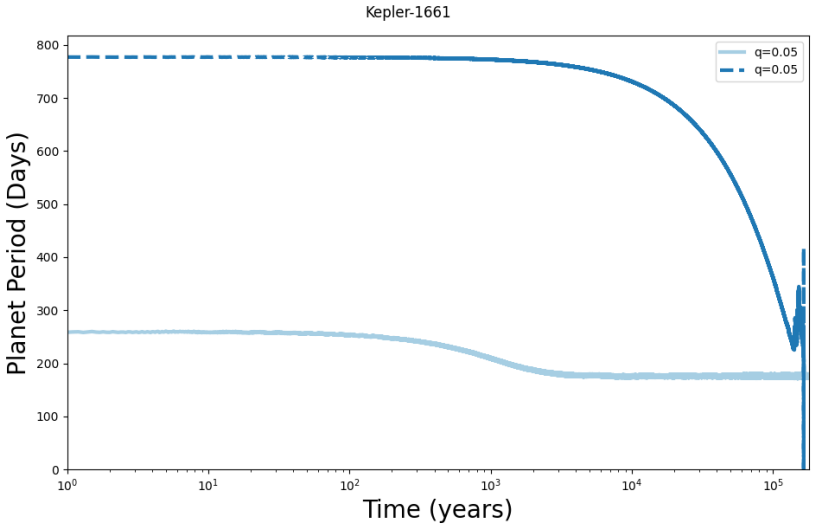

Figure 29. Second round simulation over 180,000 years after adjusting the starting positions of the inner and outer planet to allow the inner planet to migrate to its stopping position before interacting with the outer planet. Showcases an inner planet identical to Kepler-1661 b, with an outer planet of mass ratio $q = 0.05$. Stochastic forcing parameter, α set to 10^{-5}.

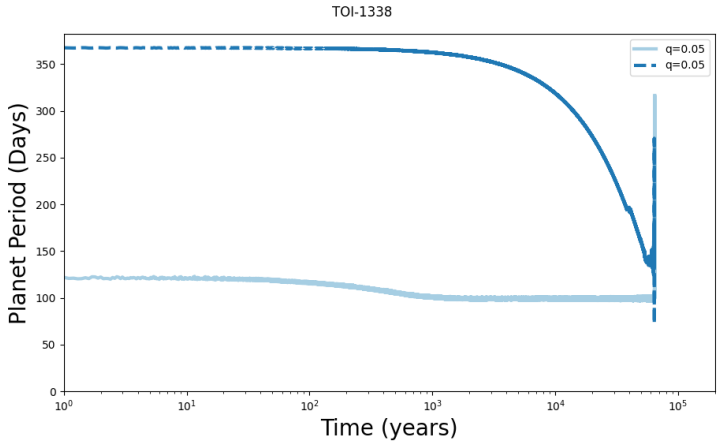

Figure 30. Second round simulation over 180,000 years after adjusting the starting positions of the inner and outer planet to allow the inner planet to migrate to its stopping position before interacting with the outer planet. Showcases an inner planet identical to TOI-1338 b, with an outer planet of mass ratio $q = 0.05$. Stochastic forcing parameter, α set to 10^{-5}.

The case of $alpha = 10^{-6}$ was more successful in producing resonant locking that remained until the end of the simulation. Kepler-38 in Figure 31 shows another locking case where it enters and remains at the 2:1 resonance. Kepler-47 in Figure 32 does not ever reach a resonance, and the migration

timescale became too long for us to simulate this process with the computational equipment at hand. Kepler-413, -453, and -1661 show remaining resonances at the end, sitting at or near the 5:2, 4:3, and 3:2 resonances. For this α value, TOI-1338 was unable to stay stable after locking into the 3:2 resonance, so we move on to simulating it at a lower α value.

The value of α clearly plays a roll in the ability for a system to reach and remain in resonance. Zeroing in on a physical, usable value for this parameter will be essential in future works as it plays heavily into correctly modeling system architectures.

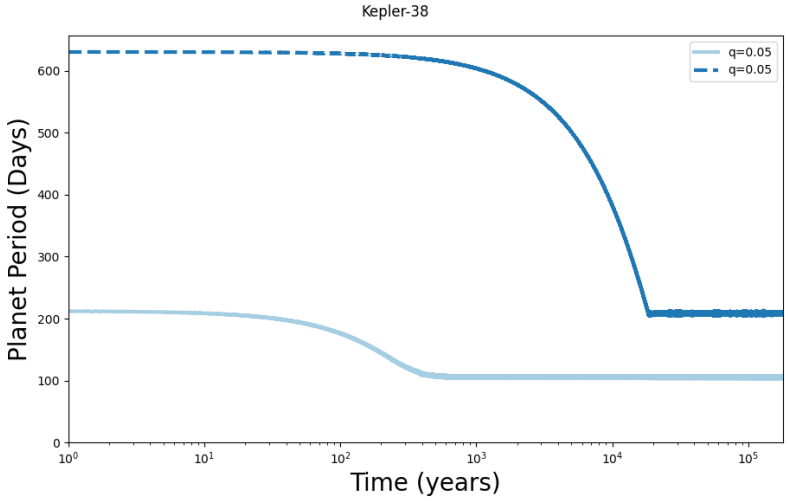

Figure 31. Second round simulation over 180,000 years after adjusting the starting positions of the inner and outer planet to allow the inner planet to migrate to its stopping position before interacting with the outer planet. Showcases an inner planet identical to Kepler-38 b, with an outer planet of mass ratio $q = 0.05$. Stochastic forcing parameter, α set to 10^{-6}.

3.3.4. $\alpha = 10^{-7}$ *Case*

With an α value equal to 10^{-7} we were able to show a stable resonant solution for TOI-1338. The outer planet migrates into a 3:2 resonance and is able to remain stable for the duration of the simulation. This is another case where order of magnitude changes in the value of the stochastic forcing parameter play into system stability.

3.4. *Establishing a Mass Transition Region for Stability*

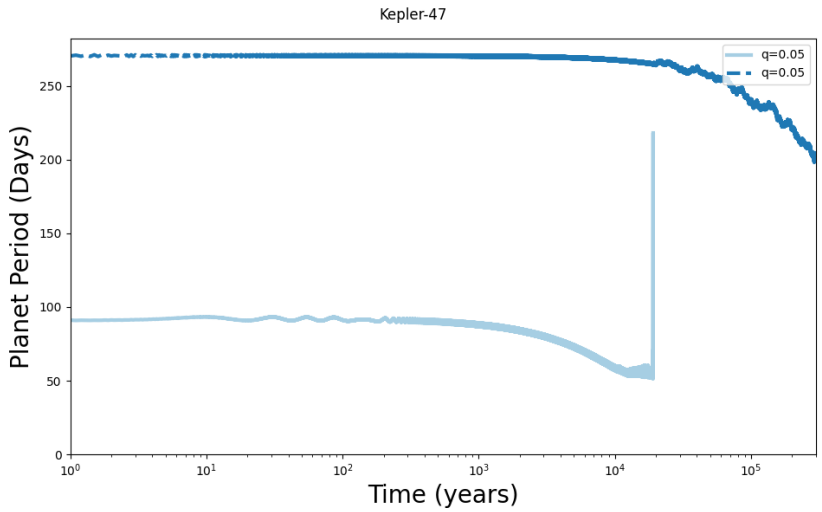

Figure 32. Second round simulation over 180,000 years after adjusting the starting positions of the inner and outer planet to allow the inner planet to migrate to its stopping position before interacting with the outer planet. Showcases an inner planet identical to Kepler-47 b, with an outer planet of mass ratio $q = 0.05$. Stochastic forcing parameter, α set to 10^{-6}.

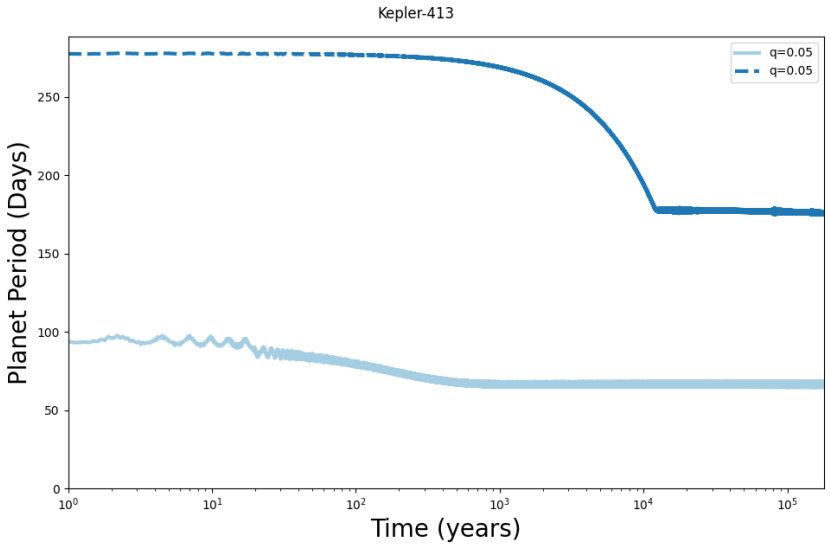

Figure 33. Second round simulation over 180,000 years after adjusting the starting positions of the inner and outer planet to allow the inner planet to migrate to its stopping position before interacting with the outer planet. Showcases an inner planet identical to Kepler-413 b, with an outer planet of mass ratio $q = 0.05$. Stochastic forcing parameter, α set to 10^{-6}.

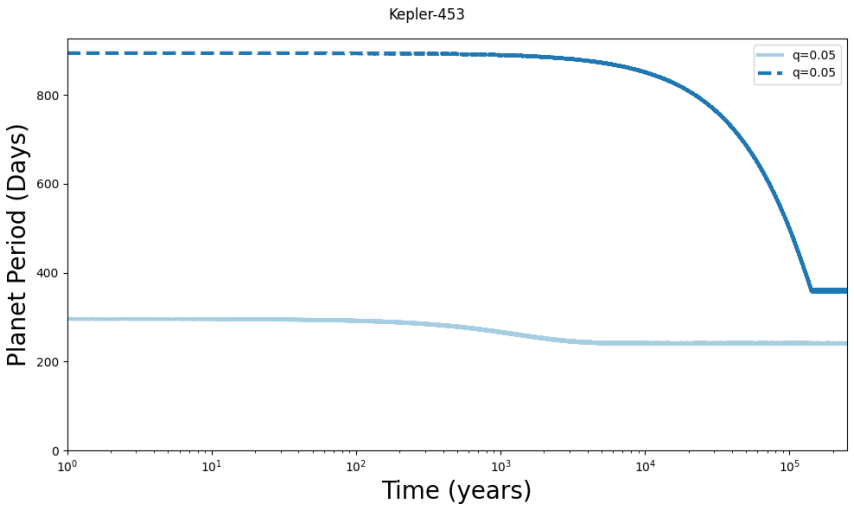

Figure 34. Second round simulation over 180,000 years after adjusting the starting positions of the inner and outer planet to allow the inner planet to migrate to its stopping position before interacting with the outer planet. Showcases an inner planet identical to Kepler-453 b, with an outer planet of mass ratio $q = 0.05$. Stochastic forcing parameter, α set to 10^{-6}.

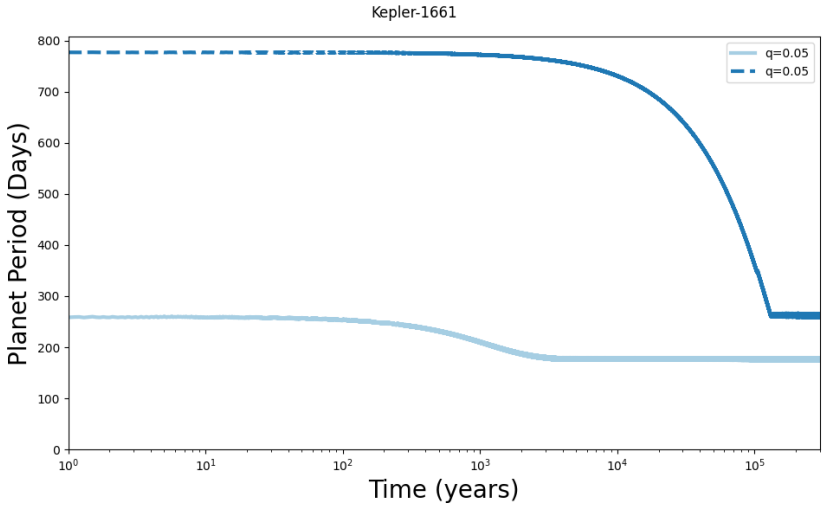

Figure 35. Second round simulation over 180,000 years after adjusting the starting positions of the inner and outer planet to allow the inner planet to migrate to its stopping position before interacting with the outer planet. Showcases an inner planet identical to Kepler-1661 b, with an outer planet of mass ratio $q = 0.05$. Stochastic forcing parameter, α set to 10^{-6}.

We have analyzed the potential for stability of an inner and outer planet in several CBP systems, varying several factors to narrow down the parameter set necessary to achieve this multi-planet

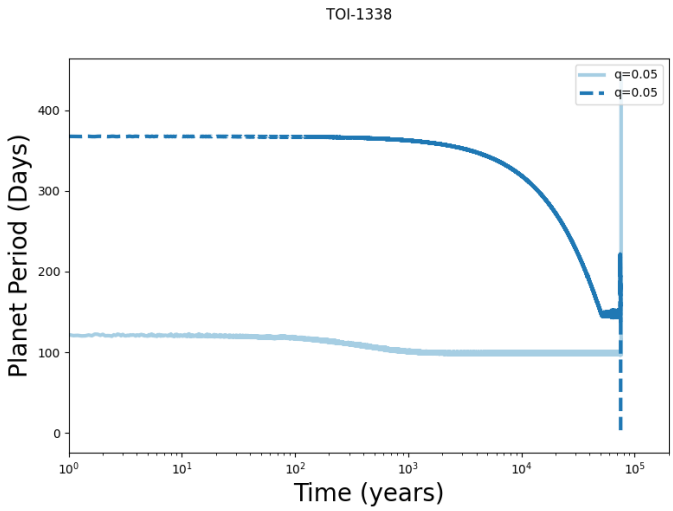

Figure 36. Second round simulation over 180,000 years after adjusting the starting positions of the inner and outer planet to allow the inner planet to migrate to its stopping position before interacting with the outer planet. Showcases an inner planet identical to TOI-1338 b, with an outer planet of mass ratio $q = 0.05$. Stochastic forcing parameter, α set to 10^{-6}.

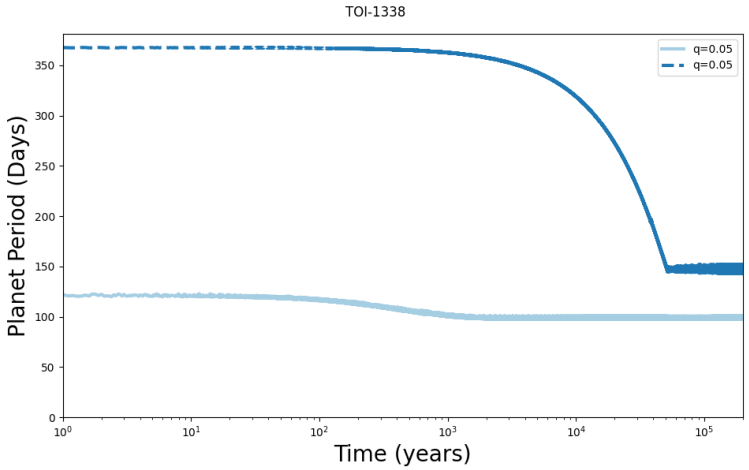

Figure 37. Second round simulation over 180,000 years after adjusting the starting positions of the inner and outer planet to allow the inner planet to migrate to its stopping position before interacting with the outer planet. Showcases an inner planet identical to TOI-1338 b, with an outer planet of mass ratio $q = 0.05$. Stochastic forcing parameter, α set to 10^{-7}.

arrangement. In order to achieve a widely applicable result, we have sought after a defining transition region based on the mass ratio, q, of the planets to find out when systems like those in our simulations move from stable to unstable.

Figure 38 shows a range of mass ratios from $q = 0.03$ to $q = 10$ for the Kepler-16 system, using 50 steps over a log scale. We chose this system because it has a low binary eccentricity, which we will contrast to Kepler-34, a high eccentricity binary. At each mass ratio, the initially outer planet is marked by blue circles, while the initially inner planet is marked by red x's. If one of these planets gets ejected during the simulation, its position on the graph drops to the bottom which corresponds to the Unstable mark on the x-axis. From $q = 0.01$ up to $q = 0.1$ we see that the system remains stable for both planets, sitting at the 2:1, 3:2, and even the 7:5 resonances. There does not appear to be a notable trend to indicate which resonance will occur, but the eccentricity of the binary and resulting planet-binary resonances likely have an influence.

Figure 39 shows the same mass ratio range, but for the Kepler-34 system. As aforementioned, Kepler-34 is a high eccentricity binary. We see both planets are stable for mass ratios up to $q = 0.4$, excluding one. For the ratios below $q = 0.2$, a 2:1 resonance is held, while from $q = 0.2$ up to $q = 0.4$, the 4:3 resonance occurs. It has been shown that planets of sufficient mass have high enough migration rates to pass through certain resonances and end up in higher order ones (Rein Year). This could be an explanation for what we see. There seems to be more of a trend here than it did in Kepler-16, but a deeper dive into the effects of binary eccentricity and planet-binary resonances would be needed to address this.

From these figures, we predict that multi-planet circumbinary systems with an inner and outer planet will require a less massive outer planet, quantitatively with $q < 1$, but more reliably, $q \leq 0.1$, in order to stay in resonance and remain stable for extended periods of time.

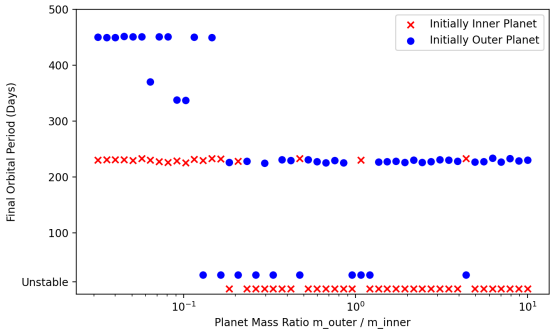

Figure 38. Kepler-16: shows the final period outcome for the initially inner and outer planets where the inner planet is modeled after Kepler-16 b, and the outer planet mass is determined by the mass ratio step as shown on the x-axis. Defines the mass ratio transition region when both planets are stable to when they are not.

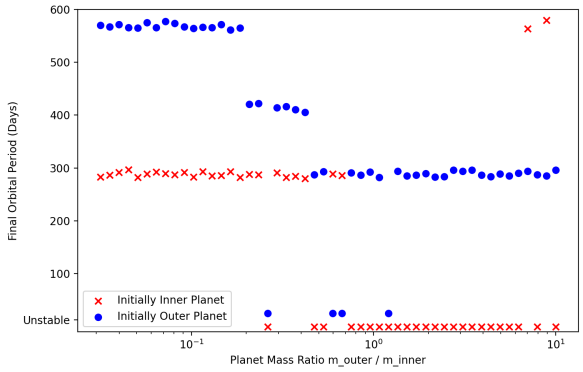

Figure 39. Kepler-34: shows the final period outcome for the initially inner and outer planets where the inner planet is modeled after Kepler-34 b, and the outer planet mass is determined by the mass ratio step as shown on the x-axis. Defines the mass ratio transition region when both planets are stable to when they are not.

4. DISCUSSION & CONCLUSIONS

4.1. *General Conclusions*

We have shown a new effect in the ability for circumbinary planets to migrate and lock into stable, resonant chains. We have probed the effects of mass relationships, resonant interactions, and stochastic forcing on this and stability of simulated multi-planet circumbinary systems. Our analysis shows that all three of these factors play a significant roll in the outcome of these systems.

We predict that a mass ratio (outer to inner planet mass) of less than 0.1 will most reliably produce stable multi-planet systems, with some exception up to a mass ratio of 0.4. Resulting resonances vary, but consistently planets that reach and remain stable in our simulations sit at the 2:1, 3:2, and 4:3 resonances. Our stochastic forcing parameter, α varies from system to system, but consistently produces stable results when the value ranges from $10^{-7} - 10^{-5}$.

To get a more clear understanding on what value of α is appropriate for which systems, a dive into the correlation between the binary eccentricity, stochastic forcing parameter, and stability of the system is needed. Our results serve as a baseline for deeper probes into the potential for currently known single CBP systems to possess an undetected outer planet. Radial Velocity surveys will be critical for detecting any potential outer planets present in these systems, as they will have longer periods and consequently a higher probability of being misaligned and thus not transiting. There is already one potential outer planet companion to TOI-1338 (Standing et al. in prep), and it fits our prediction of having a period more than two times the known transiting planet.

4.2. *In Relation to Quarles et al. 2018*

In Quarles et al. (2018), they predicted that there could be planets interior to the known CBPs, since the islands of stability shown in Figure 5 do not forbid it. Our study indicates that it would be incredibly difficult, if not impossible, for this kind of system architecture to form by migration. Based on our results, these interior planets would have to be more massive than the known planet to preserve our mass ratio transition relation and produce a stable system. A more massive planet invites more interaction with the binary meaning the fate of the planets is more likely ejection than it is collision with the star (Sutherland & Fabrycky 2016) or stability.

4.3. *Future Work*

In the future, this thesis will be converted to a paper and submitted for publishing in a journal. The results were already presented at the Triple Evolution and Dynamics conference in March 2021 in poster form (Fig. 40). On top of this project, I am also involved in a study of the migration of small, Earth-like circumbinary planets, and whether or not they migrate quickly enough to pass

through the regions of instability around binaries at resonances (e.g. 5:1 and 6:1, see Fig. 5). Much of my early work was spent on creating an automated algorithm for detecting circumbinary transits in TESS data, and I plan on circling back to this problem to help address the need to identify more circumbinary planets. I am also involved in an observational study to look at the TOI-1259 system, a giant planet orbiting a K-dwarf star with a distant White Dwarf (WD) companion. We hope to take a spectral measurement of the WD to further constrain its age, the planet's age, and test the planet disintegration theory that attributes unusually high levels of heavy metals in the upper atmospheres of WDs to their consumption of planets.

REFERENCES

Artymowicz P., Lubow S. H., 1994, ApJ, 421, 651

Bear E., Soker N., 2014, MNRAS, 444, 1698

Bromley B. C., Kenyon S. J., 2015, ApJ, 806, 98

Goldreich P., Tremaine S., 1979, ApJ, 233, 857

Kley W., Thun D., Penzlin A. B. T., 2019, A&A, 627, A91

Konacki M., 2005, in American Astronomical Society Meeting Abstracts. p. 84.02

Kostov V. B., et al., 2020, AJ, 159, 253

Lubow S. H., Ida S., 2010, arXiv e-prints, p. arXiv:1004.4137

Martin D. V., 2018, Populations of Planets in Multiple Star Systems. p. 156, doi:10.1007/978-3-319-55333-7˙156

Martin D. V., et al., 2019, A&A, 624, A68

Mayor M., Queloz D., 1995, Nature, 378, 355

Murray C. D., Dermott S. F., 2000, Solar System Dynamics

Orosz J. A., et al., 2019, AJ, 157, 174

Penzlin A. B. T., Kley W., Nelson R. P., 2021, A&A, 645, A68

Pierens A., Nelson R. P., 2013, A&A, 556, A134

Quarles B., Satyal S., Kostov V., Kaib N., Haghighipour N., 2018, ApJ, 856, 150

Rein H., 2010, PhD thesis, -

Sutherland A. P., Fabrycky D. C., 2016, ApJ, 818, 6

Sutherland A. P., Kratter K. M., 2019, MNRAS, 487, 3288

Tamayo D., Rein H., Shi P., Hernandez D. M., 2020, REBOUNDx: Adding effects in REBOUND N-body integrations (ascl:2011.020)

Windemuth D., Agol E., Carter J., Ford E. B., Haghighipour N., Orosz J. A., Welsh W. F., 2019, MNRAS, 490, 1313

Wolszczan A., Frail D. A., 1992, Nature, 355, 145

Zorotovic M., Schreiber M. R., 2013, A&A, 549, A95

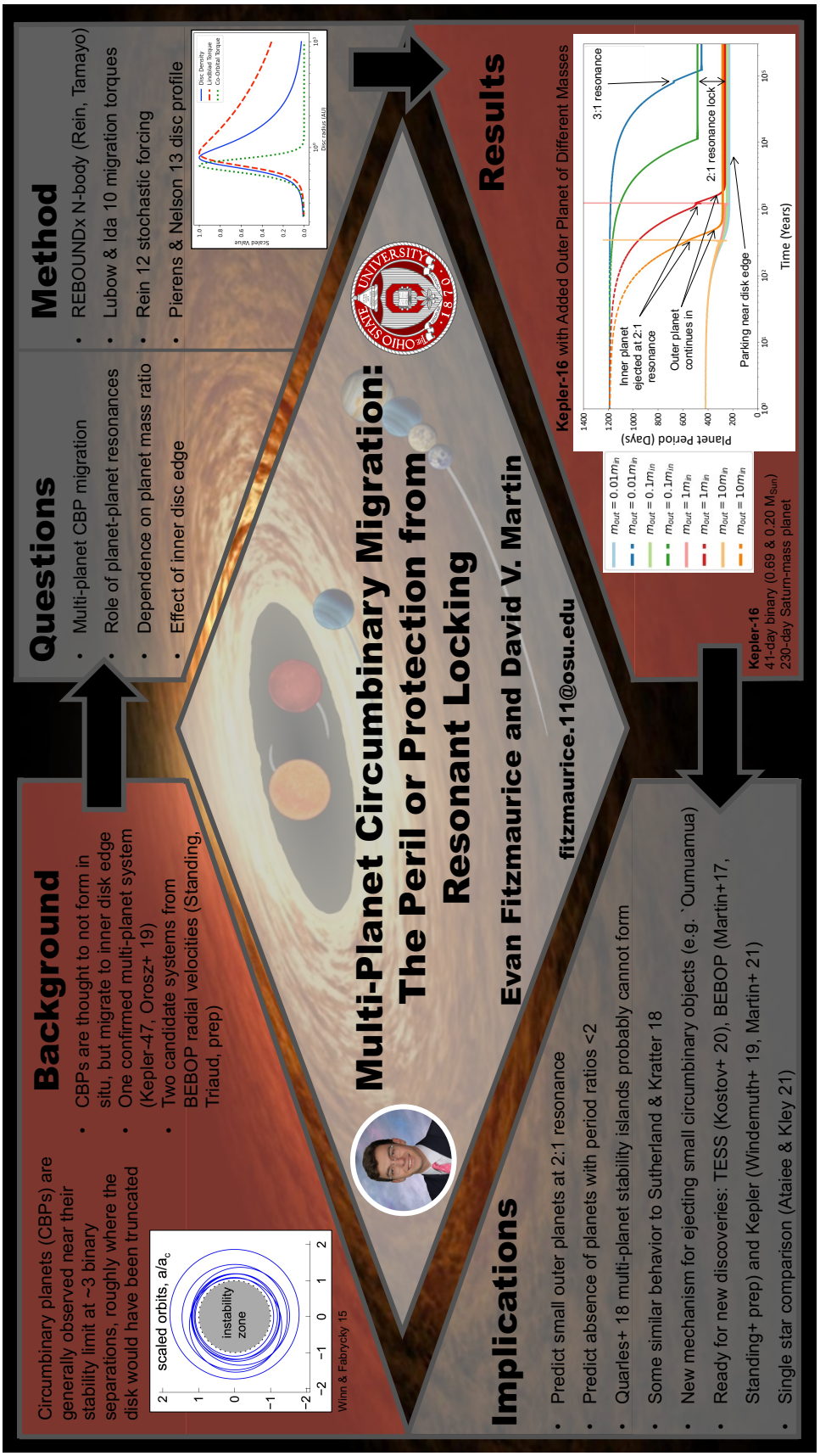

Figure 40. A poster I presented on this work at the third Triple Evolution and Dynamics conference in March 2021.